SESAR Engage KTN – catalyst fund project final technical report

Project title:	Meteo Sensors In the Sky (METSIS)
Coordinator:	Royal Netherlands Aerospace Centre (NLR)
Consortium partners:	AirHub B.V.
Thematic challenge:	TC3 Efficient provision and use of meteorological information in ATM
Edition date:	30 July 2021
Edition:	1.0
Dissemination level:	Public
Authors:	Emmanuel Sunil / NLR
	Ralph Koerse / NLR
	Stijn van Selling / NLR
	Jan-Willem van Doorn / NLR
	Thomas Brinkman / AirHub

Photo copyright ©NLR - 2021

Unless specifically mentioned otherwise, the copyright for all figures and photos in this report belongs to NLR. This does not hold for figures that have been cited from external sources.

Table of Contents

1   Abstract and executive summary

1.1   Abstract

The Meteo Sensors in the Sky (METSIS) project explores the use of drones as a wind sensor network for U-space applications. The novel concept aims to provide accurate and low-cost wind nowcasts for drones using data collected by drones themselves, i.e., 'wind nowcasts for drones by drones'. A proof-of-concept flight-test experiment was performed using four drones to determine the feasibility of the METSIS concept at low altitudes. In the current incarnation, ultrasonic anemometers were mounted to each drone to measure local winds. The flight-tests evaluated the effect of obstacle-induced wind distortion, drone motion, measurement density, and measurement errors. Additionally, wind fields estimated during the flight-tests were published in real-time to the AirHub Drone Operations Center – a functional U-space Service Provider – to demonstrate the communication of these data to real end-users. The results indicate that the METSIS concept is a promising solution for wind nowcast component of the U-space weather information service. Future research should investigate the accuracy of the concept for a wider range of scenarios than considered here, and develop the technologies needed to increase the scalability of the concept.

1.2   Executive summary

1.2.1   Background

Because of their light-weight nature, drones can be vulnerable to wind. This is particularly the case at low altitudes where both wind speed and direction can change abruptly. However, at present, real-time and accurate knowledge of low altitude wind information is limited, especially in urban areas. This limitation makes it difficult to realize the numerous anticipated applications of drones in urban areas, such as aerial photography, mapping and package delivery. The U-space weather information service aims to address this issue by making the required weather, including wind data, available to drone operators (Corus, 2019).

1.2.2   The METSIS concept and its benefits

The Meteo Sensors In the Sky (METSIS) project proposes to test the use of drones as a wind sensor network for hyper-local wind now-casting in very low level airspaces (<500 ft). The METSIS concept consists of three steps; see Figure below. This project has investigated all three steps of the concept.
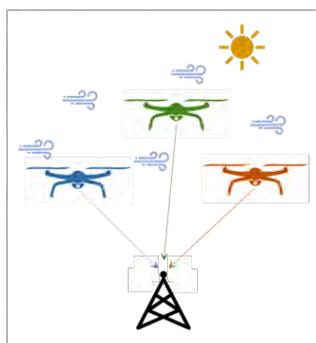
Step 1: Airborne drones measure instantaneous wind states and transmit data to a ground station
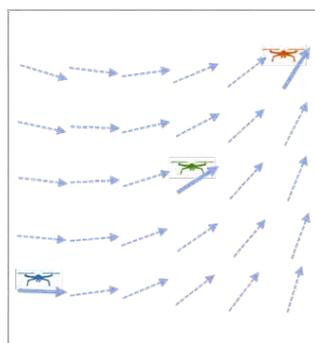
Step 2: Ground station uses the Meteo Particle Model (MPM) to estimate the wind field in real time. Here dashed arrows are MPM estimates and solid arrows are drone measurements.
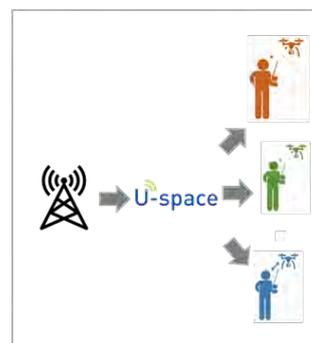
Step 3: The ground station communicates wind field data to drone operators via the U-space weather information service

The METSIS concept offers several technical and practical advantages. For drone operators, the METSIS approach has the potential to not only improve safety, but also improve flight efficiency as wind can significantly affect drone battery life and/or range. Additionally, in comparison to other approaches that make use of a dedicated measurement infrastructure such as LIDARs, the METSIS concept represents a relatively low-cost solution as the drones themselves provide the required wind measurements. This further strengthens the potential commercialization of the METSIS concept. Beyond drones, this approach for low-altitude wind measurement can also be applied to other areas of the aerospace industry, for instance for Shipboard Helicopter Operational Limitation (SHOL) analysis. Finally, METSIS has broader societal applications, e.g. safety of construction cranes, and as an additional input to national meteorological forecast systems.

1.2.3   Technical Contributions

This project resulted in the following main technical contributions:

- Wind tunnel testing of wind sensor: the accuracy of the ultrasonic wind sensor used in this project was analyzed in the NLR Anechoic Wind Tunnel.
- Meteo Particle Model extension: The MPM, which is used to estimate wind fields using drone observations, was extended to 3-dimensions.
- Development of the METSIS ground station: the ground station aggregates the data from all the drones (and wind sensors), logs the data, and uses the MPM to estimate wind fields.
- Real-time communication of wind data to a U-space Service Provider (USSP): The ground station also transmitted the MPM wind estimates in real-time to the AirHub Drone Operations Center.
- Drone-sensor configuration: four quadcopter drones were modified to mount the wind sensors onto the drones. This included modifications to the drone power supply and telemetry systems.
- Proof-of-concept flight-test experiment: A full day flight-test experiment using four drones was performed to study effects of obstacle-induced wind distortion, drone motion, measurement density, and measurement errors on the accuracy of the METSIS wind nowcasting system.

1.2.4   Conclusions

Based on the data collected during the flight-tests, the following main conclusions can be drawn:

- The flight-tests indicated that the METSIS concept is feasible in practice, i.e., that it is indeed possible to use drones as a weather sensor network for hyperlocal, low-altitude and real-time wind field estimations for U-space applications.
- When comparing the results of the experiment to the World Meteorology Organization (WMO) requirements for anemometers, the Meteo-Particle Model (MPM) showed satisfactory performance, especially during high wind speed scenarios. Therefore the MPM, which was originally developed for high altitude wind estimations for commercial aircraft, is considered suitable for low-altitude drone operations after the minor modifications made in this project.
- Answers to the main research questions of the METSIS project:
  - Effect of obstacles: static obstacles had a minor effect on overall accuracy at the distances at which drones are expected to operate from obstacles.

- o Effect of drone motion: given the low wind speeds during the experiment day, propeller induced flow had a strong negative effect on the measurements taken by the ultrasonic wind sensor during dynamic/motion scenarios. As such this research question remains inconclusive. This topic should be reconsidered in follow up research.
- o Effect of number of drones/measurement density: for the wind conditions observed during the experiment, the results indicate that a minimum of two drones are needed for the MPM to model changes in wind direction.
- o Effect of measurement error: no significant change in accuracy occurred when two different Gaussian noise models (with a standard deviation of 10% and 25% of the average wind speed during the experiment) were artificially added to measured data.
- o Communication of hyperlocal wind data to U-space Service Providers (USSPs): wind information can be transmitted in JSON format using HTTP POST. This proved to be a reliable means to communicate wind data to USSPs in real-time.

1.2.5 Recommendations for future research

Because of the promising results obtained from the flight-tests, it is highly recommended to continue this line of research as the implementation of the METSIS concept on a larger scale could result in a viable and low-cost system for hyperlocal wind nowcasts for the U-space weather information service. To this end, the following main recommendations are made to further develop this concept towards practical implementation:

- Repeat the experiment over multiple experiment days and consider more experiment scenarios to gain a more thorough understanding of system accuracy.
- Investigate methods to reduce the effect of propeller induced flow over the wind sensor during dynamic scenarios.
- Increase the scalability of the method by using indirect wind measurement techniques that do not require a dedicated wind sensor for each drone. If the wind sensor can be removed from the METSIS concept, the previous bullet point does not need to be considered for future research.
- Perform online optimization of MPM parameters to further increase accuracy.
- Future implementations should transmit wind data to USSPs in the GEOJSON data format (more widely used for weather data) via web-sockets (more scalable than HTTP Post).
- Demonstrate practical applications of hyperlocal weather information, including methods that drone operators can use to compute wind optimized routes to increase drone range/battery life.
- Explore the viability of the METSIS concept to other weather parameters such as temperature and air pressure.

2   Overview of catalyst project

2.1   Operational/technical context

2.1.1   Background

Over the past decade, drones have enjoyed tremendous media attention. The growing excitement for these new aircraft types have led many to envision a future in which large numbers of drones fly over urban areas for numerous applications ranging from aerial photography to package delivery. But before this vision for the future can become a reality, several challenges need to be tackled. One of these challenges is safe airspace integration for drones. To this end, the European Commission and SESAR have initiated the U-space program to develop the services needed to cope with the anticipated future high demand for drone flights (SESAR 2018); see Figure 1.
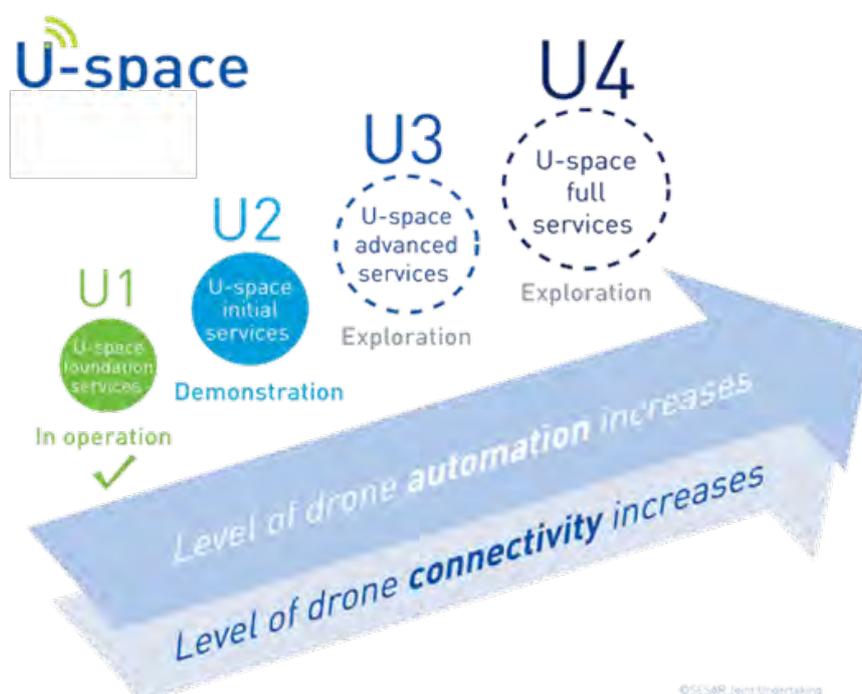
Figure 1: U-space program development phases (courtesy SESAR Joint Undertaking).

This project considers solutions for the "Weather Information" service of U-space U2 (initial services), which is intended to provide drone operators with information about the actual and forecasted weather situation (SESAR 2018, CORUS 2019). More specifically, this project focuses on a novel approach to estimate and communicate hyper-local real-time wind information to drones using data measured by drones themselves, i.e., by using drones as a wind sensor network. This approach has the potential to increase the safety of drone operations, particularly at low altitudes where wind speed and direction can vary abruptly. As such, this project focuses on Engage Knowledge Transfer Network (KTN) thematic challenge 3 in the context of drone integration:

Thematic Challenge 3: Efficient provision and use of meteorological information in ATM

2.1.2   The METSIS concept

The METSIS methodology consists of three main steps; see Figure 2.
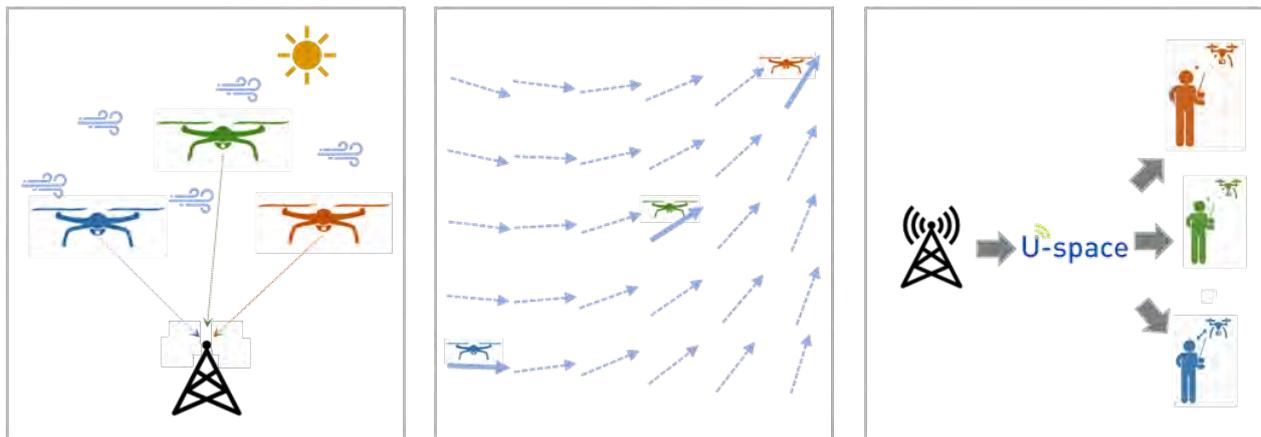
| Step 1: Airborne drones measure instantaneous wind states and transmit data to a ground station | Step 2: Ground station uses the Meteo Particle Model (MPM) to estimate the wind field in real time. Here dashed arrows are MPM estimates and solid arrows are drone measurements. | Step 3: The ground station communicates wind field data to drone operators via the U-space weather information service |

Figure 2: The three steps of the METSIS concept

In the first step, instantaneous wind speed and direction measurements are downlinked to the ground by airborne drones. Subsequently, a ground station aggregates the wind data from the individual drones, and uses the Meteo Particle Model (MPM) to estimate a 3D wind field vector map over the sensed area in real time containing both wind speed and direction (see Section 2.3.1 for more info on MPM) (Sun et al., 2018). This 3D wind field is continuously updated with new measurement data transmitted by the individual drones to ensure that any wind variations are captured. In the third and final step, the 3D wind field information in communicated to drone operators via the U-space weather information service. This wind information can be used by drone operators for determining unsafe wind areas, as well as for flight planning (before take-off) and re-planning (during flight) purposes.

The METSIS concept offers several technical and practical advantages. For drone operators, the METSIS approach has the potential to not only improve safety, but also improve flight efficiency as wind can significantly affect drone battery life and/or range. Additionally, in comparison to other approaches that make use of a dedicated measurement infrastructure, the METSIS concept represents a relatively low-cost solution as the drones themselves provide the required wind measurements. This further strengthens the potential commercialization of the METSIS concept. Beyond drones, this approach for low-altitude wind measurement can also be applied to other areas of the aerospace industry, for instance for Shipboard Helicopter Operational Limitation (SHOL) analysis, and for offshore construction activities (e.g. wind turbines). Finally, METSIS has broader societal applications, e.g. safety of construction, safety of road/marine traffic, and as an additional input to national meteorological forecast systems.

2.2 Project scope and objectives

2.2.1 Objectives and research questions

Although the METIS concept is composed of tried-and-tested ingredients, it is unclear if the accuracy of the overall method is suitable for U-space applications, particularly in the presence of static obstacles and at low altitudes. Therefore, the main objectives of this project are to:

> **Research Objectives**
>
> 1. Determine the **accuracy** of the METSIS concept in the presence of **static obstacles** to estimate low altitude winds below 1000 ft;
> 2. Determine how low-altitude wind information should be communicated to drone operators within a **U-space** system

To meet the above research objectives, NLR and AirHub B.V. performed a proof-of-concept drone flight test experiment. The experiment will aim to answer the following five research questions:

> **Research Questions**
>
> 1. What level of **accuracy** can be achieved with the Meteo-Particle Model at **low altitudes** with and without **static obstacles**?
> 2. How is accuracy affected by the **motion of the drone**?
> 3. How does the **number of drones** affect the accuracy of the wind field?
> 4. How **resilient** is the Meteo-Particle Model to **wind measurement errors** by some of the drones in the sensor network?
> 5. How can the data be **communicated in real-time** to done operators via **U-space** system?

2.2.2 Research Approach and Scope

As mentioned above, a proof-of-concept experiment was performed to validate the effectiveness of the METSIS concept. The experiment was performed at the NLR Drone Center in Marknesse, the Netherlands; see Figure 3. This unique facility has its own dedicated airspace (up to 3500 ft), and has all the permissions and equipment required to perform experimental drone test flights.

| a) Runway | b) Dedicated airspace (EHR 66) |

Figure 3: The NLR Drone Center in Marknesse, the Netherlands will be used as the test site for the METSIS experiment

To restrict the focus of the experiment towards answering the five research questions listed in Section 2.2.1, the following design choices/simplifications are proposed:

- Only **quadcopter** type drones were used;
- **2 Obstacles** obstacle types were considered during the experiment, namely a mobile trailer and a line of trees[1];

---

[1] Originally, the drone center building was also planned as an obstacle. However, time constraints caused by rain on the experiment day meant that that the scenarios next to the drone center building could not be performed.

- Only one U-space operations system, namely **the AirHub Drone Operations Center**, will be considered in this project. Nonetheless, it will be possible interface the researched methods with other U-space operations systems on the market.
- Drones measured local wind speed and direction using **onboard ultrasonic wind sensors.**

The last bullet point above indicates that onboard ultrasonic sensors are used to measure instantaneous wind speed and direction in this project. This decision was made to simplify the design of the proof-of-concept experiment considered in this work. The use of such ultrasonic sensors adds cost to the *current* implementation of the METSIS concept. But in the *future*, it may be possible to avoid the use of these sensors by inferring wind speed and direction as the difference between ground speed and airspeed using an appropriate filtering method. This aspect is considered in the recommendations section of this report; see Section 3.1.

2.3   Research carried out

2.3.1   Meteo Particle Model (MPM) and its extension to 3D

2.3.1.1   MPM

METSIS will test the use of drones as a wind sensor network for hyper-local wind field nowcasting at low altitudes (<500 ft). For this task, METSIS aims to utilize the Meteo-Particle Model (MPM), a technique for wind field estimation based on aircraft ADS-B and Mode S data and available as a Python library. Together with a research paper, this tool was developed by Junzi Sun and his colleagues at the TU Delft Communication, Navigation & Surveillance in Air Traffic Management (CNS/ATM) research group (2018). Refer to Figure 4 for an example visualization of the wind measurement, particle creation, and wind field estimation of the MPM on an XY-plane of 100 × 100 kilometers.
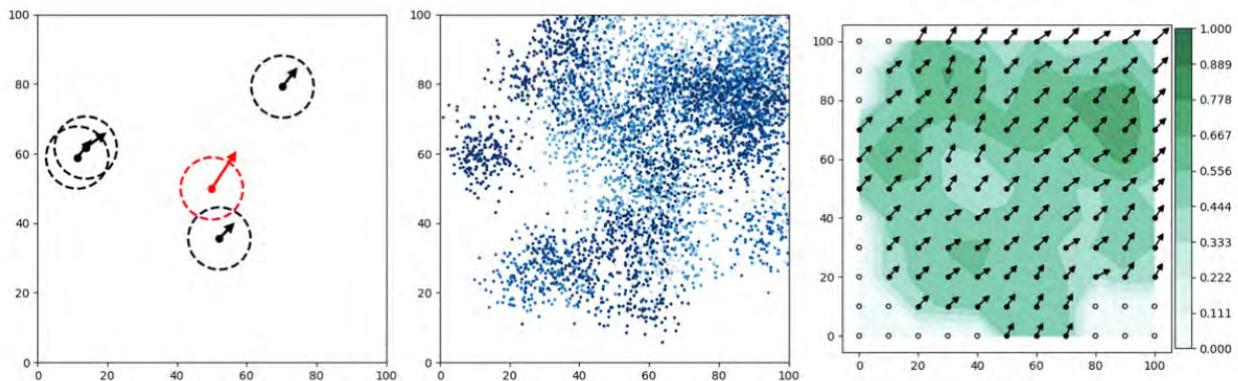
Figure 4: Wind field estimation process (measurement, particle creation, wind field estimation) of the Meteo-Particle Model (Sun, Vû, Ellerbroek, & Hoekstra, 2018)

The fundamental idea of the Meteo-Particle Model is to use a random walk process to extend weather information (modelled as particles) from aircraft flight paths to areas with little or no aircraft observations. The MPM is able to extend the weather information on a predefined grid area (X×Y×Z). It is a Monte Carlo type simulation, meaning it is a model used to predict the probability of different outcomes when the involvement of random variables is present (Kroese et al., 2014).

In MPM, particles can be considered as the information medium, propagating the wind (and temperature) measurements to surrounding areas. Over time, the particles decay according to particle age due to the probabilistic re-sampling technique. Figure 5 represents the general steps and components of the MPM, which are explained in the following subchapters.
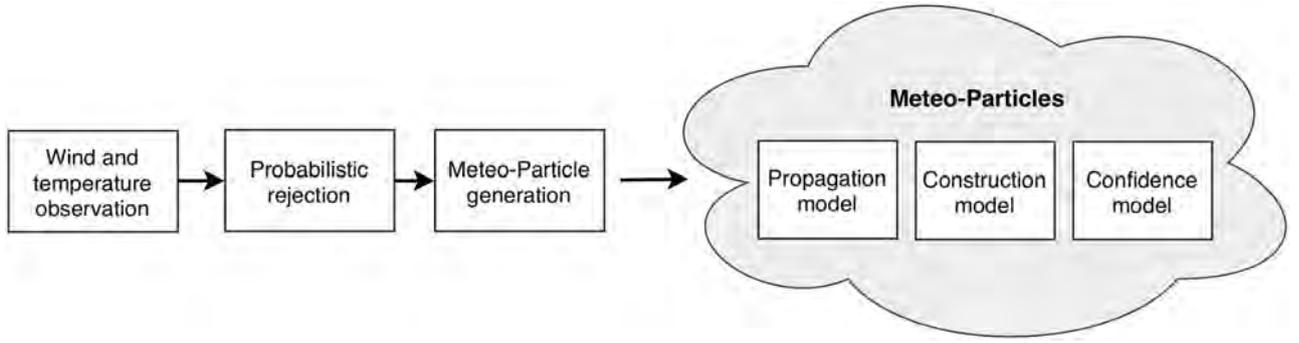
Figure 5: General steps of the MPM (courtesy of Sun, Vû, Ellerbroek, & Hoekstra, 2018)

Parameter gathering

The most important parameters that will have to be gathered are aircraft position (*x, y, z*), wind measurement vectors for west-east component *u* and a north-south component *v*. The temperature is denoted as scalar τ. The measurement array given a specific time interval is given as $[x, y, z, u, v, \tau]$.

Probabilistic rejection

A probabilistic rejection mechanism is used in order to prevent sudden variations in instantaneous wind fields due to incorrect data and random measurement errors (refer to Section 3.4). For each new measurement, there is a chance that the sample will be accepted with a probability of *p*. The mean and variance of wind and temperature states of accepted measurements from a similar altitude are computed, which are presented as (μ_u, σ_u^2), (μ_v, σ_v^2) and $(\mu_\tau, \sigma_\tau^2)$ for the *u* and *v* component of the wind and the temperature respectively. Then, the probability function is expressed as:

$$p = exp\left(-\frac{1}{2}(\bar{x} - \bar{\mu})^T\left(k_1\bar{\Sigma}\right)^{-1}(\bar{x} - \bar{\mu})\right), \text{ with:}$$

$$\bar{\mu} = (\mu_u, \mu_v, \mu_\tau)$$

$$\bar{\Sigma} = \begin{bmatrix} \sigma_u^2 & 0 & 0 \\ 0 & \sigma_v^2 & 0 \\ 0 & 0 & \sigma_\tau^2 \end{bmatrix}$$

(1)

where k_1 is being used as a control parameter to increase or decrease the acceptance tolerance of the probabilistic rejection mechanism. A low k_1 will lower the measurement acceptance.

Meteo-Particle generation

A particle, not to be confused with a physics particle, is generated when new wind measurements are observed. A particle is an information medium and consists of the position (x_p, y_p, z_p), origin (x_0, y_0, z_0), horizontal wind components (u_p, v_p), temperature τ_p and age α. *N* particles are created for each new measurement at an aircraft location. The position and wind states are measured on aircraft, hence measurement noise $\mathcal{N}$ is added to position and wind states in order to account for uncertainty of measurement data:

$$\begin{pmatrix} u_{p,i} \\ v_{p,i} \\ \tau_{p,i} \end{pmatrix} \sim \mathcal{N}\left(\begin{bmatrix} u \\ v \\ \tau \end{bmatrix}, \begin{bmatrix} \sigma_{u0}^2 & 0 & 0 \\ 0 & \sigma_{v0}^2 & 0 \\ 0 & 0 & \sigma_{\tau0}^2 \end{bmatrix}\right) \qquad i = 1, 2, \cdots, N \qquad (2)$$

Propagation model

With each iteration step, all particles will propagate according to a random walk model. Via each step of the random walk model, the particle position gets updated and particle age increases. The motion model of a particle is described with:

$$\begin{bmatrix} x_{p,i,t+1} \\ y_{p,i,t+1} \\ z_{p,i,t+1} \end{bmatrix} = \begin{bmatrix} x_{p,i,t} \\ y_{p,i,t} \\ z_{p,i,t} \end{bmatrix} + \Delta P_t$$

$$i = 1, 2, \cdots, N \qquad (3)$$

$$\Delta P_t \sim \mathcal{N} \left(\begin{bmatrix} k_2 u_p \\ k_2 v_p \\ 0 \end{bmatrix}, \begin{bmatrix} \sigma_{px}^2 & 0 & 0 \\ 0 & \sigma_{py}^2 & 0 \\ 0 & 0 & \sigma_{pz}^2 \end{bmatrix} \right)$$

where ΔP_t is the step factor and k_2 a control parameter to become more biased towards the wind direction when k_2 increases.

Probabilistic re-sampling

Re-sampling maintains the number of particles in the system according to age. First, all particles that propagated outside of the boundaries will be removed. Afterwards, all particles are sampled by age α according to the following probability function:

$$p(\alpha) = exp\left(-\frac{\alpha^2}{2\sigma_\alpha^2} \right) \qquad (4)$$

where σ_α is the age control parameter. The older a particle becomes, the more likely it is that it will be removed.

Construction model

The construction model is based on the principle that at any location (x, y, z) within the boundary area, the wind and temperature information can be reconstructed by the surrounding particles. The wind at any given position can be computed as the weighted sum of the wind state information carried by the particles. The neighbouring particles are denoted as *P*, and the wind state of particle *p* with location (x, y, z) can then be computed as:

$$\begin{bmatrix} u \\ v \end{bmatrix} = \frac{1}{\sum_{p \in P} W_p} \cdot \sum_{p \in P} \left(W_p \cdot \begin{bmatrix} u_p \\ v_p \end{bmatrix} \right) \qquad (5)$$

W_p is the weight of each particle based on the product of the two exponential functions $f_d(d)$ and $f_0(d_0)$, wherein f_d defines an exponential relationship between the weight and distance between the particle and the calculation coordinate, and f_0 defines an exponential relationship between the weight and distance of the particles from their origin:

$$f_d(d) = \exp\left(-\frac{d^2}{2C_d^2} \right) \qquad (6)$$

$$f_0(d_0) = \exp\left(-\frac{d_0^2}{2C_0^2}\right) \tag{7}$$

$$W_p = f_d(d) \cdot f_0(d_0) \tag{8}$$

where C is the control parameter that can increase or decrease the importance of f_d and f_0.

<u>Confidence model</u>

To obtain a measure of trustworthiness of the estimated wind, a confidence level model is used. The model outputs a value between zero and one, where full confidence in the estimated wind is defined by a confidence level of one.

The confidence level of wind and temperature estimates is computed as the combination of four functions:

1. Number of nearby particles (N)
2. Mean distance between particle and location of interest (D)
3. Homogeneity of wind states carried by particles (H)
4. Strength of the particles due to ageing (S)

Higher confidence levels are assigned to locations where more particles N are in the vicinity D. The homogeneity refers to the similarity of particle states and is denoted as the covariance – the measure of the directional relationship between two random variables (Dowdy, Wearden, & Chilko, 2004) – of the wind vector components of the particles:

$$H_w = \left| Cov\left(\overline{u_p}, \overline{v_p}\right)\right| \tag{9}$$

The strength parameter can be calculated as the fraction of the average particle ages:

$$S = \frac{1}{\overline{\alpha}_p} \tag{10}$$

To create a combined confidence level, the values from all four confidence functions will have to be normalised into the {0,1} range using the following scaling function:

$$s(x) = \frac{x - \min(X)}{\max(X) - \min(X)} \tag{11}$$

Finally, the final output of the confidence level model is obtained as the mean of the normalised confidence levels:

$$C_w = mean\{s(N), s(D), s(H_w), s(S)\} \tag{12}$$

<u>MPM control parameters</u>

The following table provides an overview of the most important MPM control parameters for this project.

Table 1: MPM control parameters that are of relevance to the METSIS project

Parameters	Units	Description
X-boundary	[m]	Width of the construction grid.
Y-boundary	[m]	Length of the construction grid.
Z-boundary	[m]	Height of the construction grid.
XY neighbourhood	[m]	The neighbourhood of a point is a set of points containing that point where it can move some amount in any direction without leaving the set.
Z neighbourhood	[m]	Neighbourhood in the vertical direction.
Minimal particle density	$[1/m^3]$	Minimum particle density to compute per cubic metre.
Ageing parameter	[s]	Particle ageing parameter can be used to increase or decrease the ability to track rapid local changes.
Distance weighting parameter	[m]	Increasing this parameter will increase the weight W_p of the particle in the construction model. Particles closer to their origin will contribute more to the estimation of wind at the location of interest.
XY particle random walk	[m]	Travel distance of the particle random walk on the XY plane.
Z particle random walk	[m]	Travel distance of the particle random walk in the vertical direction.
Particle wind variation	[m]	Increasing this parameter will increase the wind variation noise during particle initialisation.
Acceptance probability factor	-	Increase or decrease the measurement acceptance.
XY particle random walk factor	-	Control parameter to become more biased towards the wind direction when on the XY plane during the particle random walk motion model.
Z particle random walk factor	-	Control parameter to become more biased towards the vertical wind direction during the particle random walk motion model.

2.3.1.2   Extension of MPM to 3D

In order for the MPM to consider the vertical component of wind to properly model the turbulent flow in urban environments, a few modifications have been made to the MPM in this project. The probabilistic rejection principle (Eq. 1) is unchanged. However, the variance matrix is modified to include the vertical wind component w instead of the temperature component τ (this study is not interested in temperature measurements). Particle generation (Eq. 2) has been altered in similarly. For the propagation model (Eq. 3), an additional control parameter k_3 is introduced to control the vertical wind direction bias. The information reconstruction of Eq. 5 is extended with w without additional alterations, similar to the determination of the confidence level (Eq. 9).

2.3.1.3   Particle-ground interaction

As the original MPM was intended to be used in combination with ADS-B aircraft wind information, the effect of the ground was not taken into account. However, since this experiment will take place to altitudes up and until 100 meters. The effect of the ground has to be included. Without this alteration the model would just discard any particles that would traverse out of bounds. However as one of the boundaries in this experiment is the ground, this becomes an issue as wind interacts with the ground and the boundary layer effect becomes important since the wind speed at the ground reduces to near zero. Therefore, an alteration has been made to the way the model deals with particles hitting the ground. This is done by resetting a particle if it drops below ground level (z coordinate becomes negative) to the ground level. Thus, the z coordinate of the particle is set to 0 if it becomes negative. Another option was discussed to let the particle bounce off the ground after it hit the ground, however this would then change the properties of the particle and thus the model, causing it to behave more like a flow simulation instead of a Monte Carlo simulation. Therefore, this alternate option was deemed inappropriate as the particle approach used by MPM should not make any assumptions about the flow behavior.

2.3.2   Wind tunnel experiment design

The horizontal and vertical accuracy and precision of the ultrasonic wind sensor are examined during tests in the NLR anechoic wind tunnel while being subjected to different wind tunnel speeds and pitch angles. The resulting test data is analyzed in order to account for discrepancies during the post-experiment analysis. Discrepancies in the experiment data analysis may or may not be a result of the findings in this chapter. Figure 12 presents how the sensor-drone combination was mounted in the wind tunnel. The following independent variables were considered during the wind tunnel test:

- Three wind tunnel speeds: 6, 9 and 12 m/s
- Two drone propeller powers: 0% and 50%
- Nine angles of attack (α): $\{-2^o, \dots, 18^o\}, \ steps \ of \ 2.5$
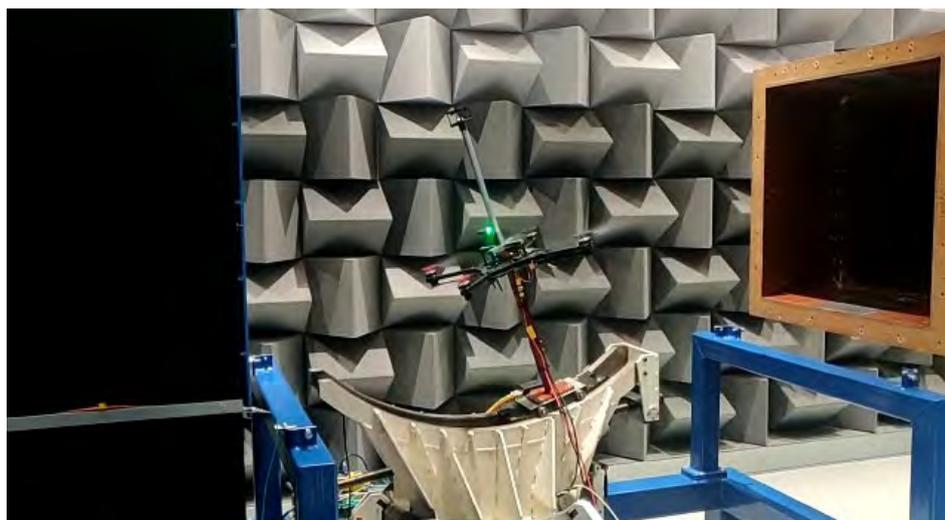

Figure 6: Wind tunnel testing of the Annemoment Trisonica Mini ultrasonic wind sensor

Following the execution of the wind tunnel test and importing the acquired data in Python, the horizontal wind speed magnitude w_{xy} is calculated using the Pythagorean Theorem of the w_x and w_y

wind components. The airflow in the anechoic wind tunnel is purely horizontal; the true measured horizontal w_{uv} and vertical wind speeds w_w will be calculated by taking into account the angle angle using trigonometry:

$$w_{uv} = w_{xy} \cdot cos(\alpha) + w_z \cdot sin(\alpha) \tag{13}$$

$$w_w = w_{xy} \cdot sin(\alpha) + w_z \cdot cos(\alpha) \tag{14}$$

2.3.3   Flight-test experiment design

The following paragraphs describe in detail the design of the flight-test experiment performed at the NLR Drone Center. The experiment was designed to answer the main research questions of this project. It should be noted that two days were originally planned for the experiment. However, signal interference issues on the first day which meant that it was not possible to guarantee safe control of the four drones at the same time. Therefore, the first day had to be cancelled. Due to team-member and facility availability during the time frame of the project, the experiment was scaled down to fit into one full day. The following paragraphs discuss the details of the experiment as executed.

2.3.3.1   Independent and dependent variables

The scenarios are kept as simple as possible and designed in such a manner that the scenarios can be equitably compared to establish a reliable proof of concept of METSIS. There has to be sufficient commonality in the design of scenarios to ensure the scenario comparisons will be made objectively. The scenarios are divided over four independent variables, which will be used to objectively measure the accuracy of the four dependent variables; see Table 2.

Table 2: Experiment independent and dependent variables

Independent variables	Dependent variables
Obstacles	Measured horizontal wind speed
Motion of drones	Measured vertical wind speed
Distances between drones	Measured horizontal wind direction
Altitudes	Measured vertical wind direction

2.3.3.2   Drone Topology

The experiment employs a predefined topology instead of free flight paths for drones. This is because predefined topologies can be pre-programmed into the drone autopilot software, which allows for autonomously flying drones and less room for human error. An equilateral triangle was selected as the drone topology in this project; see Figure 7.
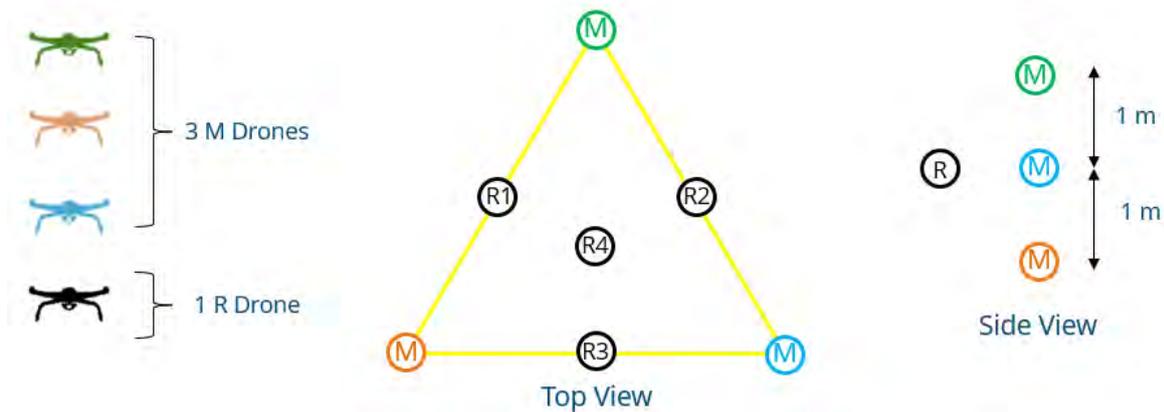
Figure 7: Drone measurement topology during the METSIS experiment

Due to the maximum availability of four drones and four sensors, three measurement drones will be used in conjunction with one reference drone - this also explains the use of an equilateral triangle as the drone topology. The measurement drones measure 3D (horizontal and vertical) wind speed and direction at the corner of the triangle, which will be fed into the MPM to construct the wind field estimations. The reference drone will measure at four different accuracy locations to determine the true wind speed and direction at specific locations. The reference drone is always static at each accuracy location to avoid random measurement errors.

In dynamic scenarios, measurement drones fly clockwise from corner to corner of the equilateral triangle resulting in a circular flight path for a constant flight speed. An altitude offset of 1 metre between measurement drones will improve safety during runs with moving drones.

2.3.3.3   Obstacles and drone motion

The scenarios are designed using a combination of static and dynamic drone motions and two different obstacle types (a small trailer and a tree line). Initially, the NLR Drone Centre building was considered as well. However, due to time limitations caused by rain on the experiment day, it was not possible to perform the corresponding scenarios. Comparing obstacle scenarios with the baseline scenario will determine how the model's accuracy is affected in the vicinity of obstacles. The hypothesis on the usage of obstacles is as follows:

- Obstacles as buildings and trees can decrease wind speeds significantly, and they often create wind distortion in their neighbourhood. Obstacles, in general, are expected to distort the wind field and reflect wind. Distortion means deformation/turbulence in wind flow (speed and direction) induced by an obstacle (Van Bussel, 2008).

The objective is to determine how much the accuracy of the METSIS concept is affected near obstacles, not to model the effect of obstacles on the wind field. Therefore, there is no need to measure wind speed and direction right next to obstacles. Instead, wind speed and direction should be measured at a distance where drones could realistically operate. The drones will fly in the wake of the trailer and trees. See Figure 8 (top side is north) for the drone's positioning relative to the tree line with a distance offset between the tree line and the centre of the drone area of about 40 metres. Wind direction during the experiment day was predominantly southwestern. For the trailer scenario, a distance offset of about 10 metres is used.
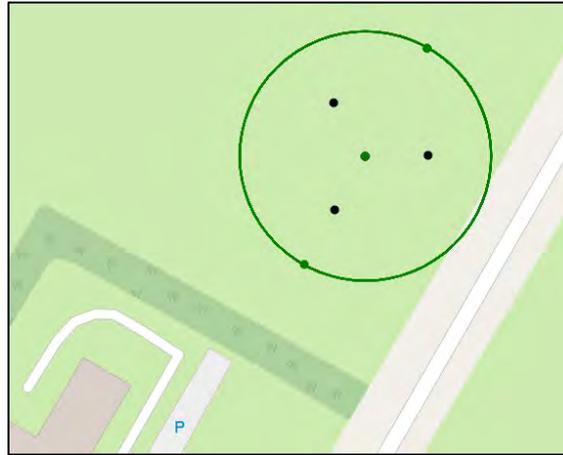
Figure 8: Positioning of the drones relative to the tree line
(black dots: reference positions, circle: dynamic measurement drone flight path)

To determine how much the accuracy is affected by flying drones compared to static/hovering drones, the scenarios are repeated using dynamic drones with a set speed of 3 m/s, which is a safe speed given the smallest triangle side length of 20 metres.

To conclude, please refer to Table 3 for the scenario definition table, in which the different scenario combinations are presented for each independent variable. Scenario 1 is the most extensive scenario, which will be the baseline scenario to compare with other scenarios. It consists of three different triangle side lengths and four altitudes. The reasoning behind the different triangle side lengths is to investigate the effect of drone density on the MPM estimations, whereas the altitudes allow the comparison between low and high altitudes. The trees scenario consists of three different altitudes, two below the height of the tree line (< 20 metres) and one slightly above. Due to time restrictions, multiple triangle sizes for the trees scenario could not be executed. The trailer is approximately ~3 metres in height.

Table 3: Scenario definition table

#	Obstacle	Triangle sizes [m]	Altitudes [m]	Speed [m/s]	Total combinations
1	-	60, 40, 20	5, 10, 20, 100	0, 3	24
2	Trailer $z \approx 3\ m$	60, 40, 20	5, 10	0, 3	12
3	Trees $z \approx 20\ m$	40	5, 10, 20	0, 3	6

2.3.3.4   Apparatus

Four Foxtech Hover 1 quadcopter-based drones were developed in this study; see Figure 9. The take-off weight of each drone was about 2.5 kg (batteries included) and unfolded dimensions of 64 × 64 × 28 cm. The additional payload weight was 1 kg, and the maximum flight duration was 15-20 minutes. The Foxtech Hover 1 uses the Pixhawk Cube Orange flight controller with 2 Global Navigation Satellite System (GNSS) and triple-redundant Inertial Measurement Units (IMU).
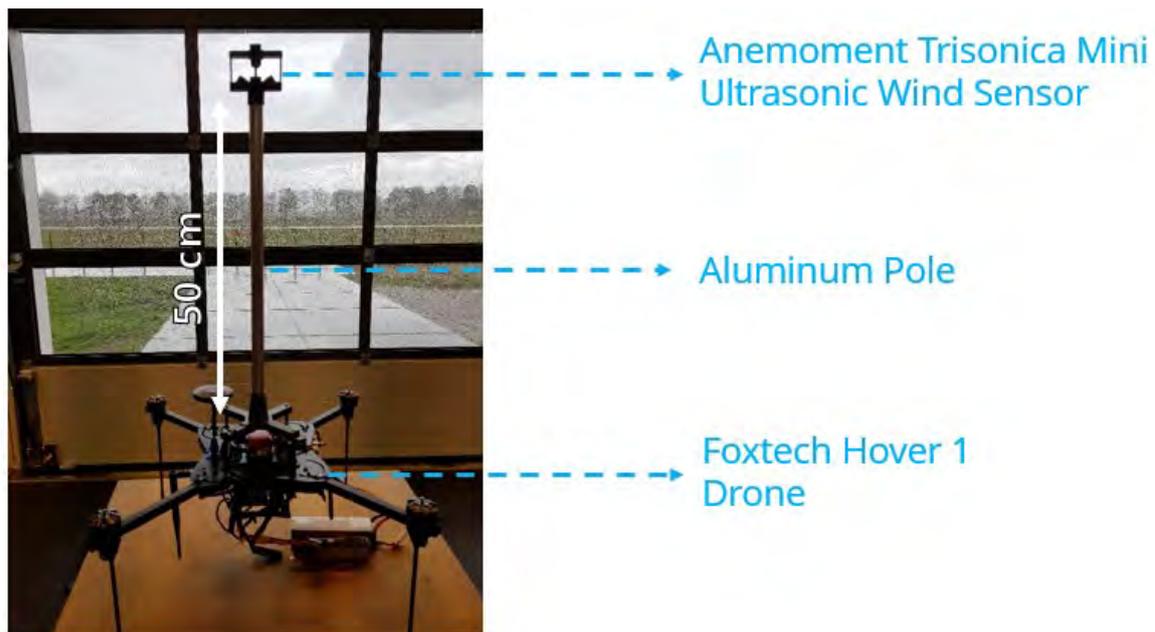
Figure 9: METSIS drone/sensor configuration

Anemoment TriSonica Mini 3D-ultrasonic anemometers were installed on top of each drone to measure the horizontal and vertical wind vectors. The anemometer sensor unit was mounted on the tip of a 50 cm aluminium pole to reduce the effect of the propeller on the wind measurements (Sasaki et al., 2021). The TriSonica Mini has the following manufacturer stated specification: wind speed range of 0-50 m/s and accuracy of ±0.1 m/s for wind speeds between 0-10 m/s. The 3D wind direction range is 360° for the horizontal direction and 15° for the vertical direction with an accuracy of ±1°. This is well within the meteorological requirements of the World Meteorological Organization (WMO), which states that using any type of modern instrumentation, an accuracy for wind speed measurements of 0.5 m/s below 5 m/s and better than 10% above 5 m/s is usually sufficient. Wind direction should be measured with an accuracy of 5° (WMO, 2014). The digital output is RS-232, a standard for serial communication transmission of data with a digital output rate between 1-10 Hz.

The software used to control the drones is the open-source ArduPilot Mission Planner software. Mission Planner enables the use of autonomous, unmanned vehicle systems for almost any vehicle and application. Furthermore, it allows the generation of pre-programmed waypoint files for the drones. This allows the reference and measurements drones to autonomously fly to the desired measurement locations and, in case of the dynamic scenarios, to autonomously fly the circular flight path at a predefined radius. The drones use ArduPilot's extended Kalman filter estimation system (Pittelkau, 2003) to estimate vehicle position, velocity and angular orientation based on gyroscopes, accelerometer, magnetometer, GNSS, barometer and ground distance measurements. ArduPilot supports MAVLink, which is a wireless messaging protocol that allows drones to communicate with ground stations.

Two-thirds through the experiment, one of the drones had a crash landing – ironically due to a sudden gust of wind during landing. The drone was repaired immediately, however, its wind sensor had suffered irreparable damage. Because of timing constraints, it was decided to continue the last third of the experiment with three drones – two measurement drones and one reference drone. This mainly affected the Trailer scenario. Nonetheless, this unexpected event did not have a significant effect on the execution of the experiment.

2.3.3.5 Measurement Procedure

Annex III presents a snippet of the Experiment Plan. This was used to coordinate the course of each scenario during the experiment. The snippet contains all the required tests to complete scenario 1. For each test, a Mission Planner waypoint file is created. These waypoint files are programmed while keeping the maximum battery life of the drones in mind for the most efficient flight time usage.

Given test 1 of the Experiment Plan, the procedure is as follows:

1. Load Mission Plan waypoint files for test 1 and start the GUI.
2. Start drones one by one.
3. Check incoming data in to the METSIS GUI; see Section 2.3.3.6 below.
4. Command drones to fly to desired position one by one.
5. Start run-in timer of 20 seconds to generate wind fields with data from measurement drones using the GUI (to allow the MPM to settle at a steady-state).
6. After 20 seconds, start reference drone measurement timer of 10 seconds.
7. After 10 seconds, reposition reference drone to the next reference location.
8. Repeat steps 6 & 7 three more times.
9. Repeat steps 5 to 8 for the dynamic scenario.
10. Repeat steps 5 to 9 for each triangle size and altitude combination.
11. Land the drones, change batteries and prepare for the next test.

2.3.3.6 Data flow and networking

Figure 10 presents the METSIS data flowchart, which is an overview of the entire data network. The data of the four drones are transmitted by a 433 MHz transmitter and received at the four Drone Ground Stations (DGS). Each drone transmitter-receiver pair has its own channel ID and operates at a slightly different frequency to reduce interference. Another transmitter-receiver pair will transfer the sensor data from all four sensors to a single Sensor Ground Stations (SGS).
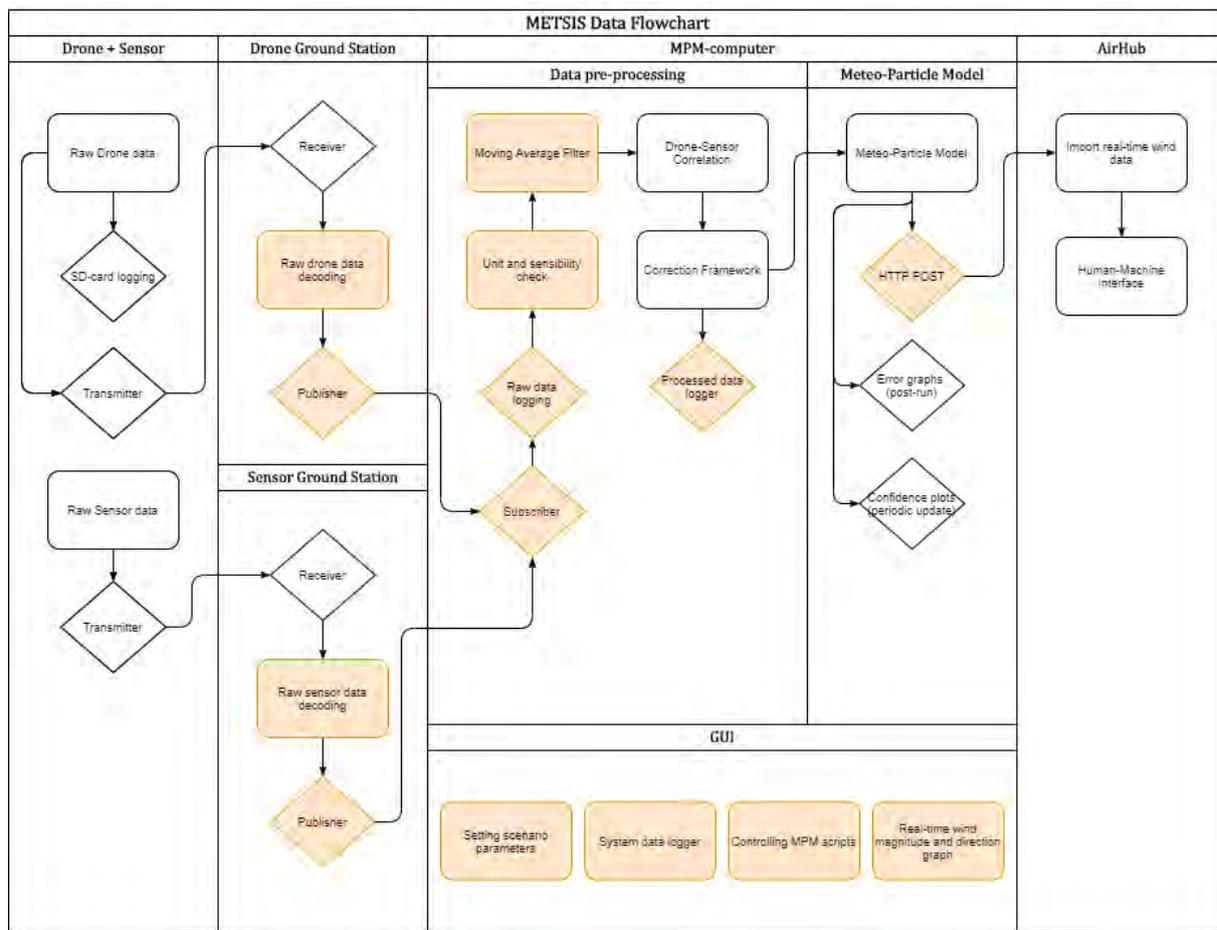
Figure 10: METSIS data network flowchart

Using Python package "PyZMQ", a python implementation of the well-known ZeroMQ messaging library, the data from all ground stations was transferred to the MPM-computer via a Publisher/Subscriber pattern. PUB-sockets (ground stations) are connected to a SUB-socket (MPM-computer) which is bound to a computer network port number. Due to multiple PUB-sockets, the data of specific ground stations may drown out other ground stations. Therefore, data is interleaved ("fair-queued") so that no single publisher drowns out the others. This PUB/SUB-pattern was also used for script-to-script object transfer at the MPM-computer.

Logging

The data required for answering the research questions are obtained using a quantitative data collection method during the METSIS experiments. All data is automatically organized in a separate folder for each scenario combination. In addition to logging the raw drone and sensor data, the processed data will be logged as well. According to the WMO, it is desirable to sample the wind signal data every 0.25 seconds to be able to measure wind gusts (WMO, 2014). Therefore, the raw drone and sensor data will be logged at a frequency of 4 Hz. The processed data will be logged at a frequency of 1 Hz, as this is the MPM-update rate (see Section 3.2.6). The approximate logging time per scenario combination is 2 minutes, providing a sample size of 480 data points per drone. The reference drone will sample for 10 seconds × 4 reference drone positions ≈ 160 data points.

By adding the vertical wind component to the MPM, the minimal required parameters for 3D wind field estimation using the MPM are:

- Position, on a Cartesian coordinate system (x, y, z)

- o Converted from the longitude, latitude and altitude measurements of the drone GNSS.
- Horizontal and vertical wind vectors in Earth-Centred, Earth-Fixed (ECEF) frame (u, v, w)
  - o Converted from the w_x, w_y, w_z wind components of the sensor in the body frame using drone velocity, attitude and course correction.

The drone and sensor output the parameters as depicted in Table 4 and Table 5. In addition, the drone and wind sensor output data such as temperature and accelerations, which will be logged in the same file for possible follow-up research. Using the drone airspeeds, course, and attitude angles, a coordinate transformation will be applied to the sensor wind measurements to derive the true $u, v,$ and w meteorological wind components in the ECEF frame from the measurements in the body-frame of the drone, where a positive u wind is from the west, and a positive v wind is from the south. Vertical wind direction is given by w, which is positive when wind travels upwards.

Table 4: Logged drone parameters

Parameter	Symbol	Unit
ID	*ID*	-
Timestamp	*t*	[Y-M-D h:m:s:ms]
Latitude	*lat*	[deg]
Longitude	*lng*	[deg]
Altitude Above Sea Level (ASL)	*z*	[m]
Horizontal speed	v_{xy}	[m/s]
Vertical speed	v_z	[m/s]
Course angle	φ	[deg]
Pitch angle	θ	[rad]
Roll angle	ϕ	[rad]
Yaw angle	ψ	[rad]

Table 5: Logged wind sensor parameters

Parameter	Symbol	Unit
ID	*ID*	-
Timestamp	*t*	[Y-M-D h:m:s:ms]
x-axis wind component	w_x	[m/s]
y-axis wind component	w_y	[m/s]
z-axis wind component	w_z	[m/s]

After the raw drone and sensor data has been correlated and transformed to ECEF, the resulting data (a collection of approximately four measurements per drone) is logged as well. This 'processed data log' can be used to re-run the MPM after the experiment:

- Timestamp [Y-M-D h:m:s:ms]
- Latitude & longitude [degrees]
- Altitude [m]
- Corrected *u* wind component [m/s]
- Corrected *v* wind component [m/s]
- Corrected *w* wind component [m/s]

Unit and sensibility check

After the drone and sensor data has been logged, it is subjected to an automatic unit and sensibility check. The unit and sensibility check is a simple Python script that will remove a measurement from the data flow if it is not within predefined value limits due to unreliability in wireless serial communication. This ensures, first and foremost, the proper functioning of the drone/sensor correlation and the reference frame transformation, which depends on the drone position and attitude. It functions based on the following principle:

- Documents what the script expects:
  - All required drone and sensor variables.
  - Sensible values within predefined limits; see Table 6.
- Check whether sensor and drone data are conforming to the expectations.
- Data that fails the test will be removed from the data flow.

Table 6: Unit and sensibility check limits

Drone data	Drone limits {min, max}	Sensor data	Sensor limits {min, max}
lat	{-90, 90}	w_x	{-15, 15}
lng	{-180, 180}	w_y	{-15, 15}
z	{-10, 200}	w_z	{-10, 10}
v_{xy}	{0, 20}		
v_z	{-10, 10}		
φ & ψ	{0, 2π}		
θ & ϕ	{-0.5π, 0.5π}		

Moving median filter

To compensate for the noisy wind sensor data, a simple moving median filter will be applied to the incoming data stream. Much like a moving average filter, a moving median is the median of a set amount of consecutive measurements (window size) in a time series (Hyndman, 2009). A moving median is conceptually similar to a moving average, except that a single outlier in the moving average greatly affects the mean (Stone, 1995). The median is calculated by sorting all the numbers in the window and selecting the middle number. Given a window *x* of *n* values, if the number of values is odd, the number in the middle of the window is the median *m* (Eq. 15). Else, if the number of values is even, then the median is the simple average of the middle two numbers (Eq. 16). The moving median filter is applied to the instantaneous w_x, w_y, and w_z sensor measurements.

$$m = x_k; \qquad k = \frac{(n+1)}{2} \qquad\qquad (15)$$

$$m = \frac{(x_k + x_l)}{2}; \qquad k = \frac{n}{2}; \quad l = \frac{n}{2} + 1 \tag{16}$$

Due to the chaotic nature of wind, a small window size of five samples has been used for this experiment with the aim to retain fluctuations in wind velocity. Figure 11 depicts a comparison of such raw data versus moving median sensor data.
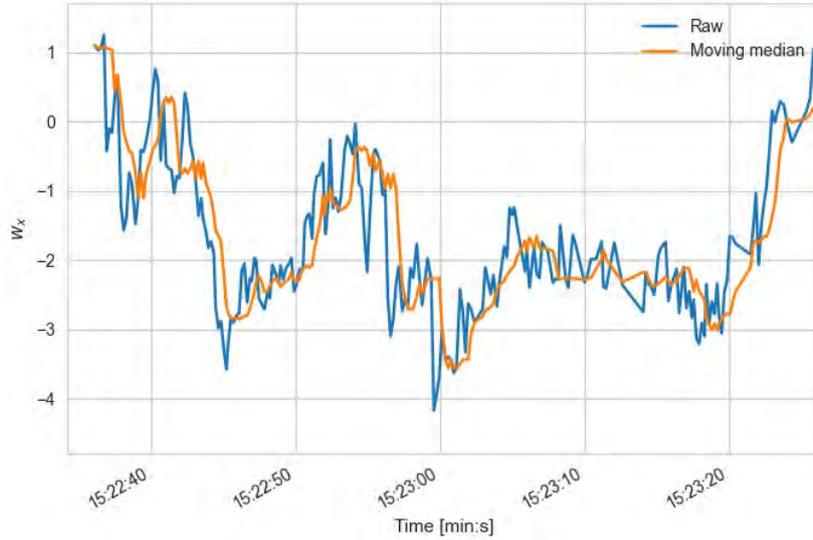

Figure 11:Applied moving median filter example on wind sensor w_x measurements

Drone/sensor correlation

A drone and sensor measurement timing difference make it difficult to combine the two incoming data streams of drones and sensors. Therefore, a drone-sensor correlation function is written in order to match the timing difference by interpolating the drone states to the wind sensor time. In short, given two known drone measurements at $t = 1$ and $t = 3$ given by coordinates (x_0, y_0) and (x_1, y_1) and one sensor measurement at $t = 2$, the interpolated measurement y at sensor time x is defined as (x = 2 in this example):

$$y = y_0 + (x - x_0)\frac{y_1 - y_0}{x_1 - x_0} \tag{17}$$

Reference Frame Transformation

The reference framework transformation utilizes the position, attitude, drone velocities and wind information from the drone-sensor correlation to take into account the motion and attitude effects from the drones as the wind sensor measures wind in its body reference frame. Furthermore, a correction for the drone and sensor offset is applied, given the length of the aluminium pole of 50 cm. The correction framework outputs the meteorological u, v, and w wind components in the ECEF-frame. Two reference frames are considered: the body reference frame of the drone and the earth reference frame. See Annex V for more details on the reference frame transformation.

MPM

The update rate of the MPM is set to 1 second. Given the drone and sensor datalink frequency of 4 Hz, a collection of ideally four measurements per drone will be sent to the MPM during each update.

The MPM samples the data from the three measurements drone and sequentially performs the following steps:

1. Collect wind components and position variables
2. Run the probabilistic rejection mechanism (Eq. 1)
3. Generate particles and add measurement noise to particle states (Eq. 2)
4. Update existing particles using the random walk motion model (Eq. 3)
5. Re-sample the particles to maintain the number of particles according to age (Eq. 4)

Data from the reference drones travel a different route. The MPM is able to reconstruct wind information at any given location. Given the reference measurement locations, the MPM construction model is called upon (Eq. 5-8). The MPM will return wind information at the reference drone locations during a reference measurement period. The script will calculate the error between the MPM estimations and the reference drone measurements in terms of MAE and save it for post-experiment analysis.

Table 7 gives an overview of the MPM control parameter values that were used during the experiment. These values were determined by a preliminary PSO using simulated drones and a simple Computational Fluid Dynamics (CFD) model of the experiment area.

Table 7: MPM control parameters used during the experiment

Parameters	Units	Value
X-boundary	[m]	(0, 140)
Y-boundary	[m]	(0, 140)
Z-boundary	[m]	(0, 170)
XY neighbourhood	[m]	18.199
Z neighbourhood	[m]	25.698
Minimal particle density	$[1/m^3]$	0
Ageing parameter	[s]	180
Distance weighting parameter	[m]	30
XY particle random walk	[m]	14.227
Z particle random walk	[m]	23.500
Particle wind variation	[m]	0.2
Acceptance probability factor	-	29.465
XY particle random walk factor	-	0.268
Z particle random walk factor	-	0.165

HTTP POST to AirHub API

Every 30 seconds, the estimated 3D wind field in the MPM-specified boundary area is transmitted to the AirHub Drone Operations Center Application Programming Interface (API) via a Hypertext Transfer

Protocol (HTTP) POST request method. A large collection of wind vector estimations is collected in a JSON file (a data-interchange format). The same architecture could be used to POST the data to other U-space service providers.

Graphical User Interface

The GUI is designed specifically for the METSIS experiment. A screenshot of the main screen is presented in Figure 12. The GUI offers the following functionalities during the experiment:

- Set scenario parameters
    - Scenario number
    - Triangle size
    - Altitude
    - Speed
- Set control parameters
- System data logger to log measurement start and stop times and reference drone start and stop times. This allows us to re-run the experiment virtually using the exact timeframes that were used during the experiment.
- *Measurement drone ready* button, which starts the MPM Python scripts.
- *Reference drone ready* button, which starts a reference drone measurement.
- Visualization of the four sensor-measured wind magnitudes and directions.
- *Check data* button to check if data is coming in from all four drones and sensors.
- *Cancel test* button, which resets the scenario in case of a test failure.
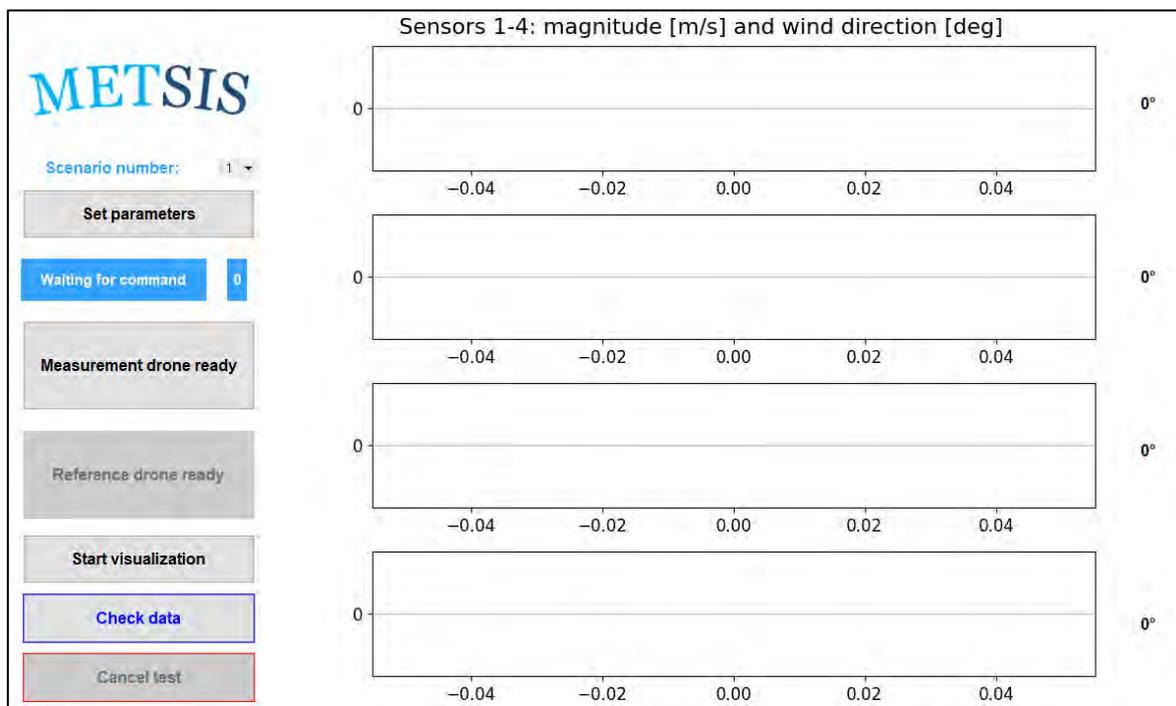

Figure 12: The METSIS GUI main window

2.3.3.7   Post-experiment data analysis method

The following paragraphs explain the metrics used to analyze the data, and how this is used to answer each research question.

Performance metric

As recommended in the Guidelines for Nowcasting Techniques (WMO, 2017), good performance metrics are the MAE and the Root Mean Squared Error (RMSE). In terms of RMSE, the effect of large errors has an increasingly large effect, due to the squared error. Thus, RMSE is sensitive to outliers (Chai & Draxler, 2014). The meteorological accuracy requirements for any type of modern wind sensors are depicted as a MAE of 0.5 m/s below 5 m/s and better than 10% above 5 m/s, as stated by the WMO (WMO, 2014). Therefore, the choice has been made to only consider MAE. For the first research question – the effect of obstacles – the MPM performance will be quantified in terms of the MAE of the following dependent variables:

1. Horizontal wind speed [m/s]
2. Vertical wind speed [m/s]
3. Horizontal and vertical wind direction [deg]
   a. Wind direction in degrees {0, 360} relative to the true north. 180 degrees wind is southerly wind, and 90 degrees wind is easterly wind.
   b. Vertical wind direction on the XZ and YZ planes, where the XZ plane defines the North-South component and the YZ plane the East-West component of the vertical angle.

The remaining research questions will only consider the horizontal wind speed and direction, as mainly the research question regarding obstacles is expected to have a significant effect on the vertical errors.

MAE is, as the abbreviation implies, defined as the average of the absolute errors. Errors are the difference between the observed values and the true values (ISO, 1994). This metric is used to verify experimental results on an absolute scale using the same units. Moreover, 3D wind magnitude will be quantified in terms of the Mean Absolute Percentage Error (MAPE) when the observations get larger (WMO, 2017), which provides a better understanding of the magnitude of the error in relation to the true observed values (Botchkarev, 2018). A high MAE would imply that the model estimates are not close to the true observed values. Model improvements can be evaluated by using the MAE as a frame of reference. The formula to calculate MAE is:

$$MAE = \frac{1}{N} \sum_{i=1}^{N} |e_i - o_i| \qquad (18)$$

where:

- N is the number of observations from the reference drone for a specific scenario combination.
- e are the MPM estimated values.
- o are the reference wind sensor observed values.

Low altitude accuracy measurement with and without obstacles

Using two types of drones (measurement and reference drones), data from three measurement drones will be fed into the MPM to estimate the wind fields. Accuracy will be determined by

comparing the MPM estimate to measurements from a reference drone. MAE between MPM wind field estimates and reference drone measurements at the four accuracy locations can be used to quantify accuracy (see Figure 13). To determine the effect of static obstacles, the accuracy of scenarios with and without static obstacles will be compared, given that other scenario parameters are kept constant. A higher MAE for the scenario with a static obstacle would imply static obstacles negatively affect the MPM accuracy.
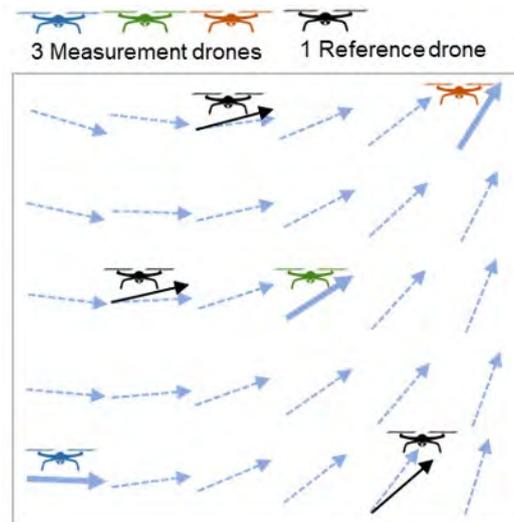

Figure 13: METSIS accuracy measurement principle using two types of drones

Effect of drone motion

By comparing the static and dynamic scenarios, the effect of drone motion on the MPM accuracy can be determined. The dynamic drone scenarios with speeds of 3 m/s will be compared to static drone scenarios.

Effect of measurement density

There are two methods to measure the effect on accuracy by drone density. Firstly, by artificially deleting one measurement drone from the set post-experiment. An increase in MAE would show the importance of a dense area of drones for accurate estimations. In contrast, a negligible decrease suggests the MPM propagation model functions well on areas with minimal measurement activity. Secondly, the MPM propagation model can be evaluated by increasing the triangle size and comparing the accuracy of the scenarios with different equilateral triangle side lengths.

Effect of measurement errors

The probabilistic rejection mechanism – or, the MPM's resiliency to measurement errors – can be validated by adding artificial random noise to measurement drones. Every wind sensor measurement will be subjected to Gaussian noise. They describe a commonly occurring distribution of samples influenced by random disturbances, such as random measurement errors. The probability density function for a Gaussian distribution is defined as:

$$p(x) = \frac{1}{\sqrt{2\pi\sigma^2}} e^{-\frac{(x-\mu)^2}{2\sigma^2}} \tag{19}$$

where μ is the mean and σ the standard deviation. Two degrees of Gaussian noise will be used with a standard deviation of 10% and ~25% of the average measured wind speed.

2.4 Results

2.4.1 Wind tunnel results

This section provides the results of the wind tunnel tests used to analyze the accuracy of the Anemoment Trisonica Mini wind sensors used in this study. Figure 14 visualises the w_{uv} error distribution of test samples per pitch angle for the three wind tunnel speeds considered. The distance between the second quartile line of the boxplots and the actual wind tunnel speed (dashed line) indicates the accuracy, while the distance between the minimum and maximum values of a boxplot indicates the variability or precision. Negative pitch angles show an unusual low accuracy, which is likely due to an obstruction of wind by the wind sensor's frame. In addition, drone rotor power has a noticeable effect on the accuracy due to propeller downwash, where the effect is more significant during the 6 m/s wind tunnel speed, indicating that the propeller downwash has a stronger effect during lower wind speeds. While examining the spread, the precision of the wind sensors is decreasing slightly with increasing wind tunnel speed.
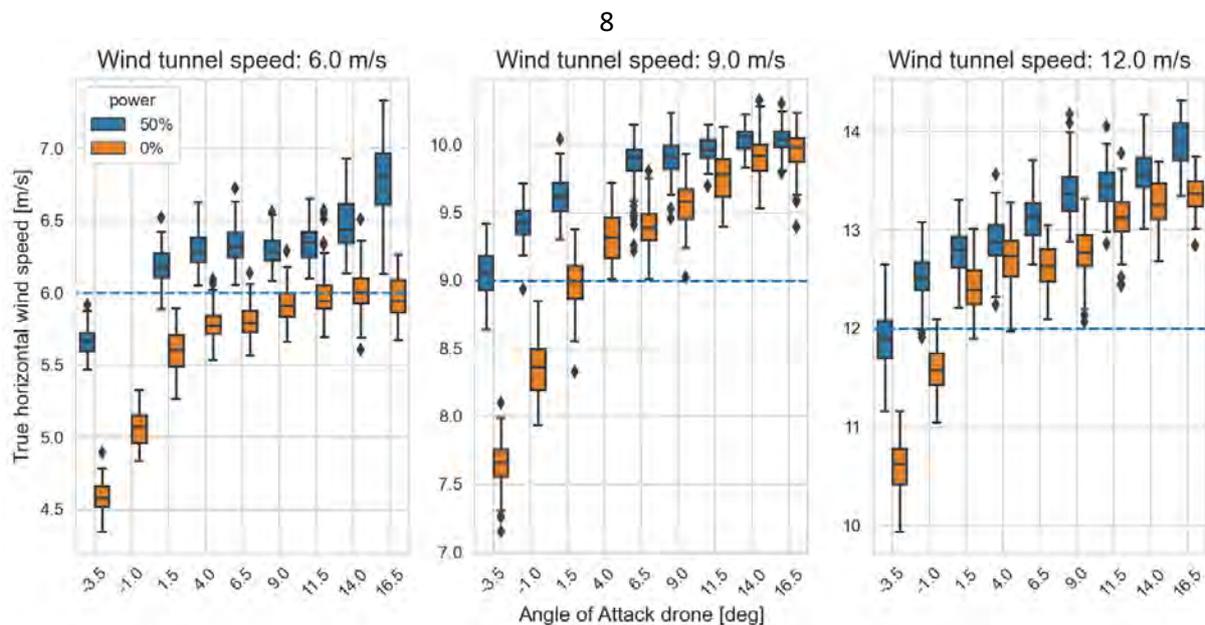
Figure 14: Error distribution of sensor horizontal wind speed to wind tunnel speed

Figure 15 depicts the vertical w_w error distribution. Due to the wind tunnel stream being purely horizontal, the sensor vertical wind measurement should ideally be equal to zero. As with the horizontal accuracy, vertical accuracy degrades with angle of attack and wind speed, but at an increased rate. The precision is high during the 6 m/s wind tunnel speed without rotor-induced downwash. An increase in wind tunnel speed and drone rotor power signifies a slight decrease in precision.
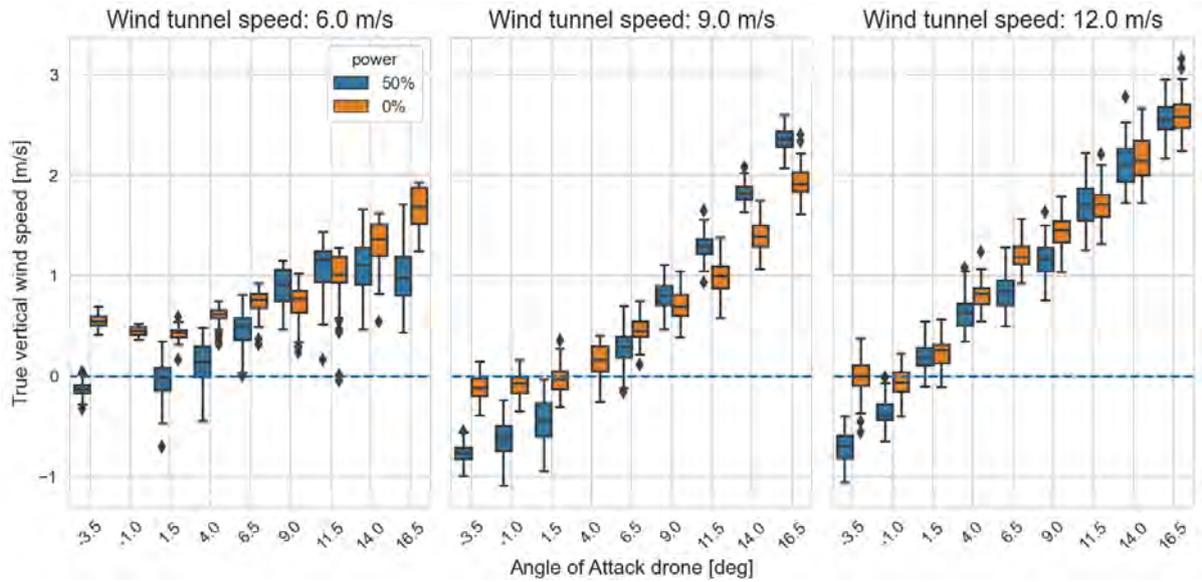
Figure 15: Error distribution of sensor vertical wind speed to wind tunnel speed

Figure 16 presents the RMSE for the horizontal (left) and vertical (right) wind speeds. At higher angles of attack, turbulence is most likely changing the local wind field at the sensor, causing different horizontal and vertical wind speeds relative to the free stream. This means that the sensor output at higher angles is not very useful for the MPM, and the drone airspeed will likely have an effect on the MPM accuracy. The vertical RMSE is bigger than desired and likely not that useful for dynamic drone scenarios, where corrections for roll and pitch angles are applied due to drone motion.
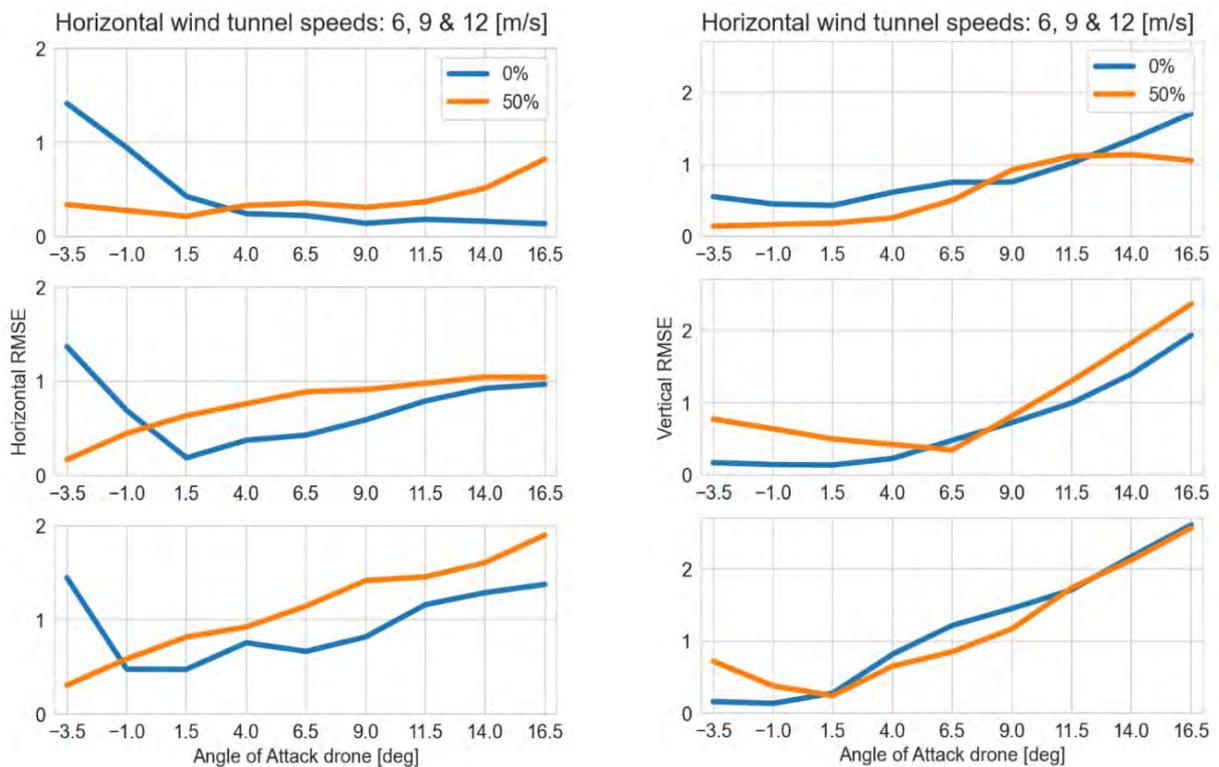
Figure 16: Wind sensor RMSE against drone pitch angle for horizontal (left) and vertical (right) direction

Based on the above results, the following main conclusions can be drawn about the performance of the selected wind sensor:

- Accuracy degrades with angle of attack in both horizontal and vertical directions, which is likely due to induced turbulent flow around the wind sensor by wind obstruction of the sensor frame. A wind tunnel smoke test could prove this hypothesis.

- Propeller-induced flow mainly adds a more significant component to the measured wind during low pitch angles and low wind tunnel speeds. This suggests that propeller-induced flow will have an increasingly negative effect on accuracy during low wind scenarios. Nonetheless, it does not seem to have an effect on precision, which is presumably due to constant rotor power. During the experiment, rotor power constantly changes according to external forces acting on the drone, which in return reduces precision due to an increased amount of random error.

- Sensor precision is lower than desired, especially in the vertical direction with propeller-induced flow. This results in noisy wind measurements and, therefore, a moving median filter is applied to the incoming data stream to account for expected random errors.

In relation to the true wind tunnel speeds (≥ 6 m/s for horizontal and 0 m/s for vertical), the magnitude of the error is greater in the vertical direction, resulting in less accurate measurements.

2.4.2   Flight test results

2.4.2.1   Overall results

Annex IV presents an overview of all the wind magnitude and angular errors – in terms of MAE (Eq. 18) –, including the average wind velocity ($\bar{v}_w$) for each scenario combination during the experiment. As stated by the meteorological requirements of the WMO, using any type of modern instrumentation, an accuracy for wind speed measurements of 0.5 m/s below 5 m/s and better than 10% above 5 m/s is usually sufficient. Wind direction should be measured with an accuracy of 5° (WMO, 2014). Comparing these requirements to the METSIS experiment results, the MPM slightly underperforms, but shows overall very promising results. This is especially true for experiment scenarios during high wind speed conditions. For scenarios with an $\bar{v}_w$ of > 5 m/s, the accuracy in terms of MAPE is ~88%. The one scenario with a $\bar{v}_w$ of > 6 m/s shows a promising 94.3% accuracy on the 3D magnitude. In comparison to accuracy results (84.5% to 95.7% without modelling 3D wind fields) from Thielicke et al. (2021), the MPM estimates are fairly accurate. The average horizontal and vertical angular MAE for the baseline scenario are respectively 15.6° and 19.3°, with the lowest achieved errors being 8.0° and 8.6°. Comparing these results to Thielicke et al. (error of 2.6° to 8.0°), the estimations of the MPM are once more fairly reasonable.

Figure 17 presents a bar chart overview of the average wind magnitude MAE and horizontal and vertical angular MAE per scenario. A minor increase in wind magnitude error is perceived for the obstacle scenarios, when compared to the baseline. The tree line scenario shows a significant increase in angular error on the XZ-plane.
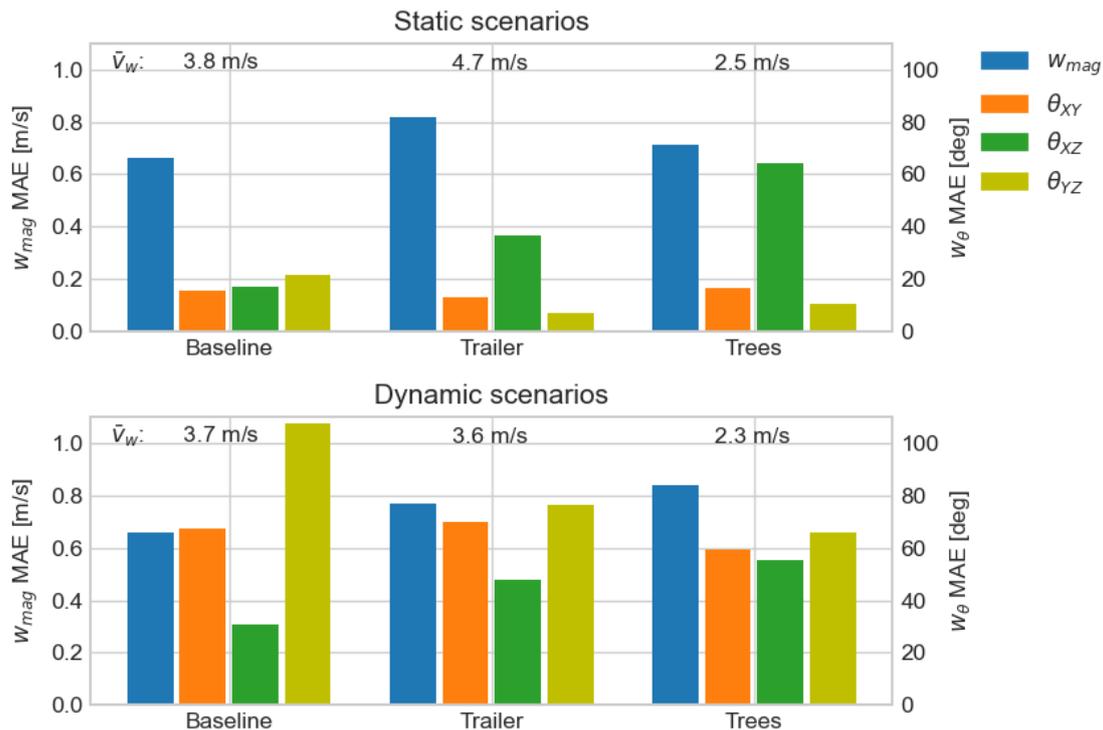
Figure 17: METSIS experiment average 3D wind magnitude and angular MAE per scenario

Given the data in Annex IV and Figure 17, there appears to be a relationship between the angular errors and the average wind speed. Using Python's *statsmodels* library, three multivariate Ordinary Least Squares (OLS) regression analyses are performed to statistically analyze the effect of the average wind speed on the MAE. The full OLS results are visible in Annex VI. To summarize, the average wind speed seems to have a significant effect on the angular errors, in addition to the tree line scenario having a significant effect on the vertical angular error. According to the OLS, no independent variable significantly affects the 3D wind magnitude error. Plotting the line of best fit for the (combined) vertical and horizontal MAE over the average wind speed from a simple linear regression model suggests that the average wind velocity has a larger impact on the angular errors than the obstacle types; see Figure 18. Nonetheless, there is insufficient data available with low wind speeds to make a definitive conclusion, and the effect of obstacles cannot be excluded. The following paragraph will determine the true effect of obstacles, while taking into consideration the effect of the average wind speed on the angular errors.
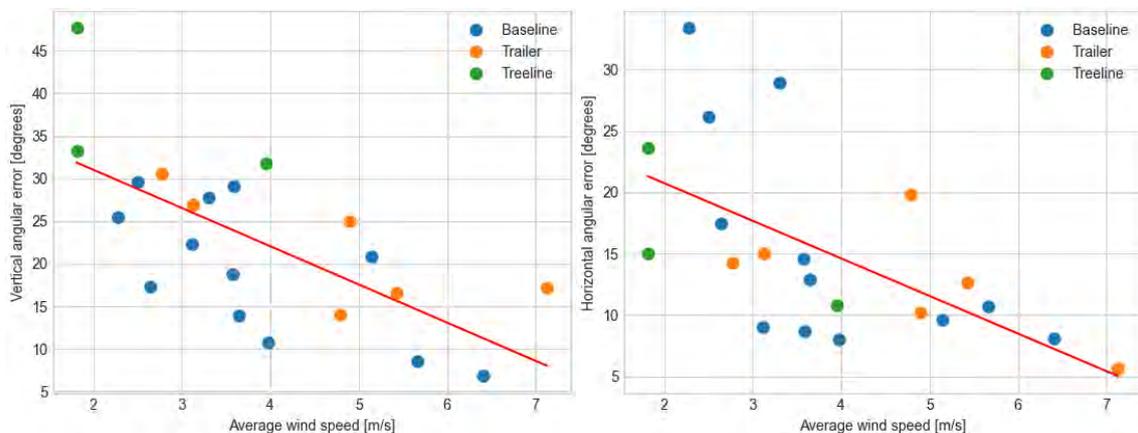

Figure 18: Line of best fit (red line) for the average vertical (left) and horizontal (right) angular errors over the average wind speeds per scenario

2.4.2.2   Research question 1: Effect of static obstacles

This section will provide an answer to RQ1: What level of accuracy can be achieved with the Meteo-Particle Model at low altitudes with and without static obstacles? Only static scenarios are considered. The baseline scenario will be compared to the trailer and tree scenarios for all common altitudes and triangle sizes. Boxplots provide an indication the error distribution of the measured errors for all dependent variables, namely: horizontal and vertical wind speed and direction. Lower error indicates a better performance of the Meteo-Particle Model. The following paragraphs will analyse the effect of obstacles on the MPM horizontal and vertical magnitude and angular errors.

Horizontal Magnitude Error
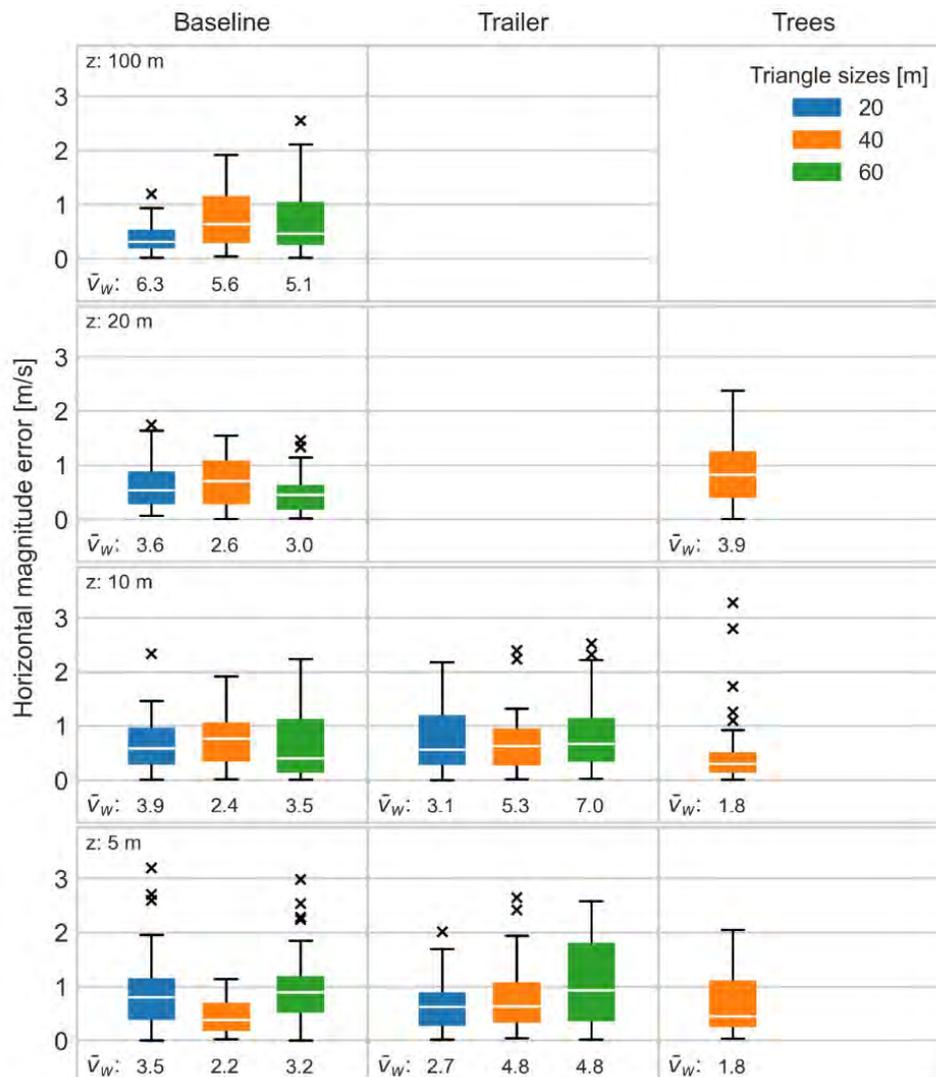
Figure 19: Horizontal wind magnitude error overview – static

Figure 19 visualizes the horizontal wind magnitude error distribution of every static scenario combination. Columns denote the different obstacle types, rows represent the different altitudes, and boxplot colors represent the triangle sizes. As concluded from the wind tunnel analysis, a low wind speed negatively affects the measurement precision and accuracy due to propeller-induced flow. Therefore, the average horizontal wind speed $\bar{v}_w$ measured by the reference drone during a specific scenario combination is annotated at the bottom of the boxplot. Rotor power of the four drones – and, therefore, propeller downwash – are not synchronized, which results in an increase in random

measurement error and dissimilarity between measurements of the different drones. This could explain the relatively lower precision during the experiment, in comparison to the wind tunnel analysis. Triangle sizes and altitudes have a negligible effect on the error difference. Comparing the baseline to the trailer scenario, the trailer had no noticeable effect on the horizontal magnitude error. The wind distortion effect of trees on the wind is clearly visible; the lowest average wind speeds are measured below the tree line (< 20 m). Nonetheless, the visible obstruction of wind during the trees scenario shows no noticeable increase in error. To summarize, the MPM performs well within the presence of static obstacles compared to the baseline scenario for the horizontal wind speed.

Vertical Magnitude Error
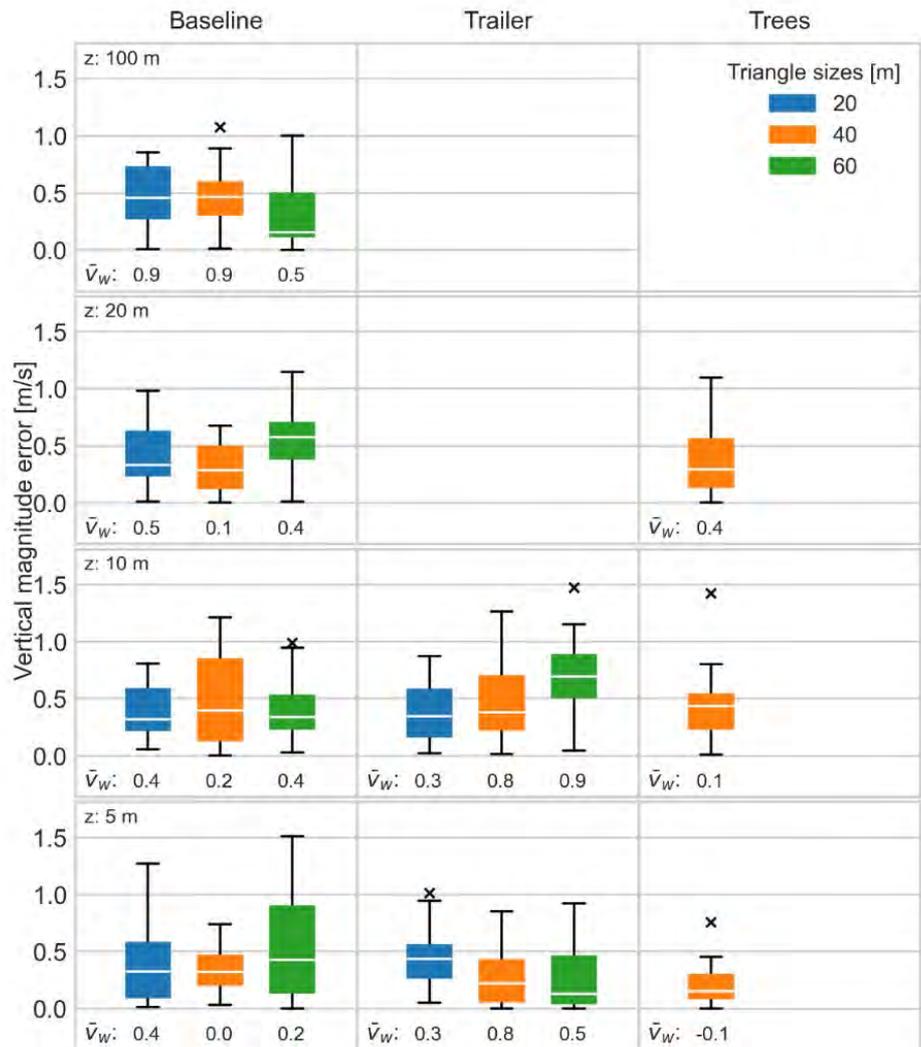
Figure 20: Vertical wind magnitude error overview – static

An overview of the vertical wind magnitude error for the static scenarios is given in Figure 20. The average vertical wind speed $\bar{v}_w$ measured by the reference drone is annotated. In general, the error is high, likely due to the low average vertical wind speeds, where the propeller-induced turbulence plays a more significant role. Interesting is the negative vertical wind for the tree line scenario at 5 meters altitude. This indicates a turbulent wind flow after an obstacle, which may cause fluctuations in drone attitude states (Wang et al., 2019). Nonetheless, no increase in error is perceived near obstacles. Thus, the MPM performs well given the clear effect of trees on the wind. However, these

results are somewhat inconclusive due to the effect of propeller-induced turbulence, increasing the random measurement error during low average wind speeds.

While the error might seem high compared to the magnitude of the vertical wind, plotting the reference drone measurements over the MPM estimates - see Figure 21, static baseline scenario, triangle size 20 metres and altitude 20 metres - shows that the MPM slightly underestimates the average vertical wind speed, but is not able to model instantaneous changes in vertical wind speed. This is true for most other scenario combinations as well. Referring back to the construction model of the MPM, the wind and temperature information can be reconstructed by computing the weighted sum of the wind state information of the surrounding particles. By decreasing the XYZ neighbourhood parameters – and, therefore, reducing the effect of the weighted sum – might prove to assist the MPM in modelling instantaneous changes. Furthermore, reducing the ageing parameter allows the MPM to more easily track rapid local changes in wind estimations, while losing stability for the larger airspace.
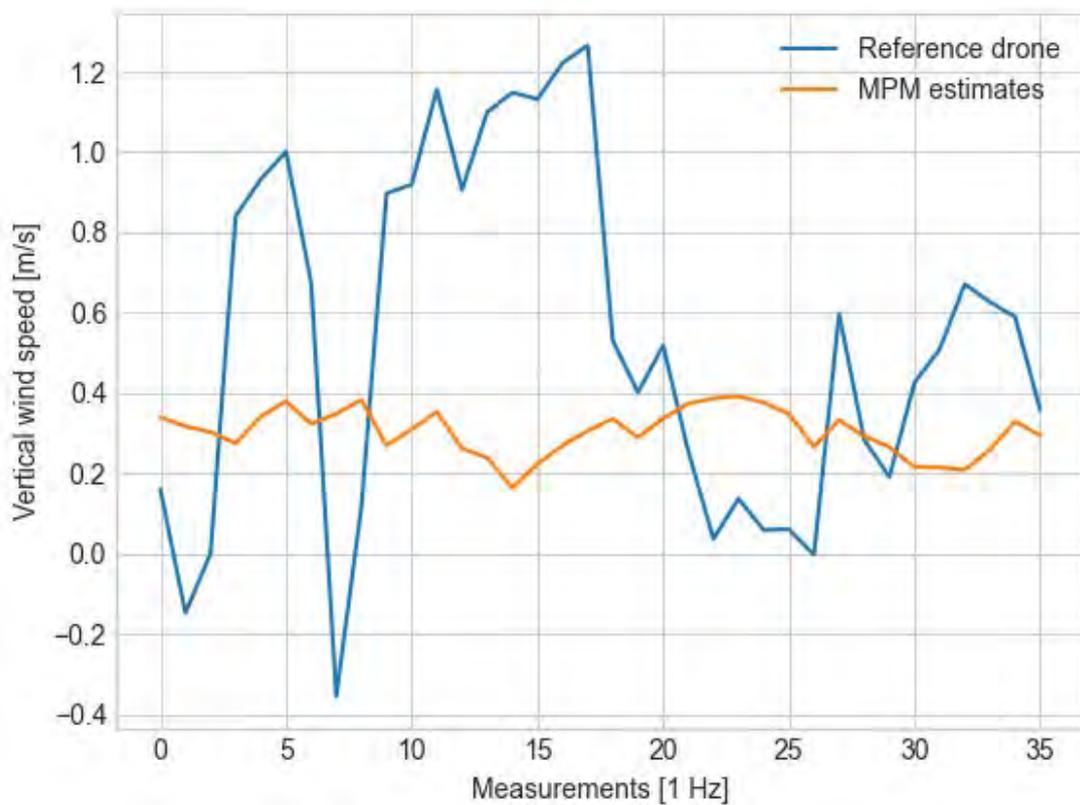
Figure 21: Comparison of the vertical wind magnitude of the reference drone and MPM estimates for one scenario combination

Horizontal angular error

The static scenario horizontal angular error distributions are given in Figure 21. Using the results from Thielicke et al. (2021) as a reference, where a wind angular error between 2.6° to 8.0° is realised, the horizontal angular errors are practicable for scenarios with $\bar{v}_w$ > 4 m/s with an average error of 12.6°. Altitudes below the tree lines show a recurring trend regarding the relative error, indicating the effect of the tree line on the angular wind. In contrast to the results for the vertical magnitude error, the tree line scenario shows an increase in error. The trailer has no significant effect on the angular error. Consistently, there is room for improvement in regard to measurement quality during low wind speed scenarios, especially when the obstruction of wind behind substantial obstacles is such an important factor in urban areas.
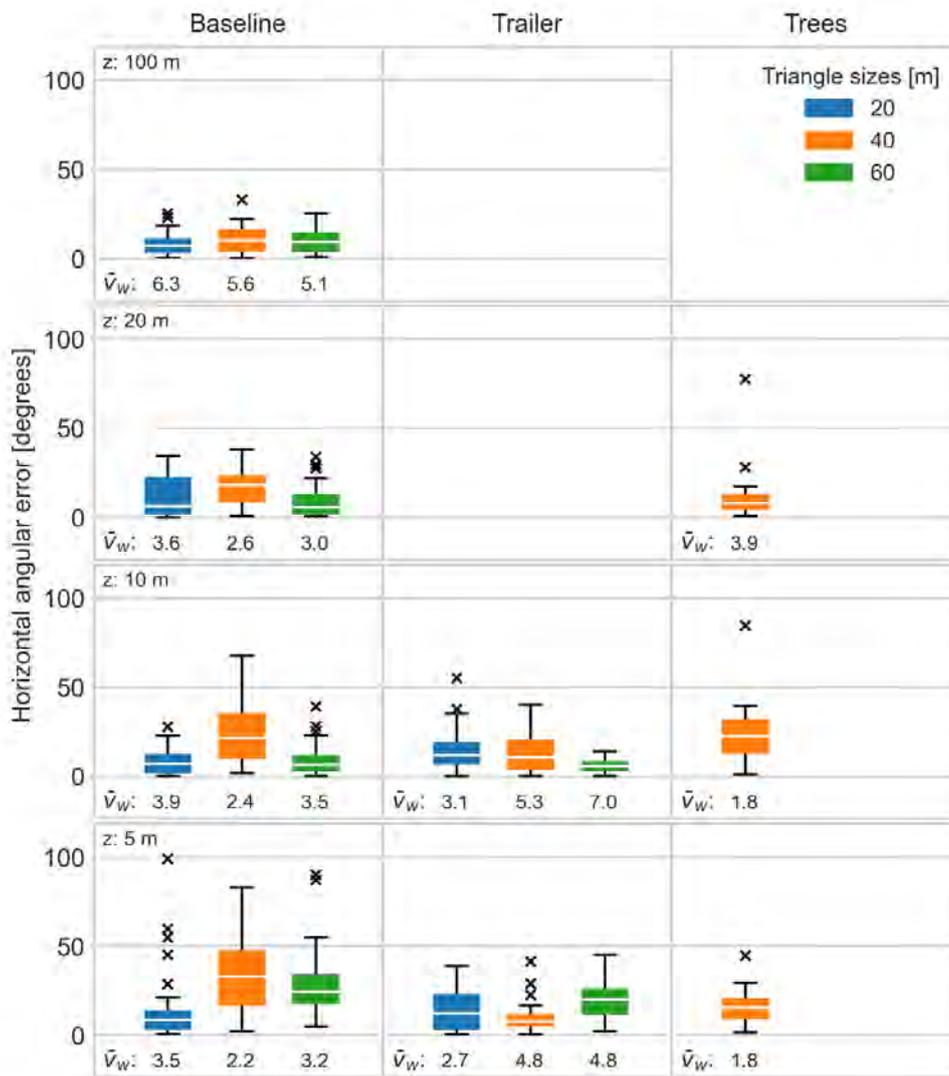
Figure 22: Horizontal wind angular error overview – static

<u>Vertical Angular Error</u>

Figure 23 presents the vertical angular error distributions on the XZ and YZ planes. The average measured wind speed of respectively the XZ and YZ wind magnitude measurements of the reference drone are annotated at the bottom of the boxplots. For the trailer and tree line scenarios, the drones were positioned north of the obstacles. The figure shows that the MPM performs well during high average wind speed scenarios. Subsequently, the tree line scenario's XZ plane shows a significant decrease in precision (random error). Similar to the horizontal angular error, it can be concluded that the vertical angular errors are highly dependent on the wind speed and, concurrently, the increased effect of wind distortion and propeller-induced turbulence. With better quality measurements, the error might reduce. This needs to be examined further.
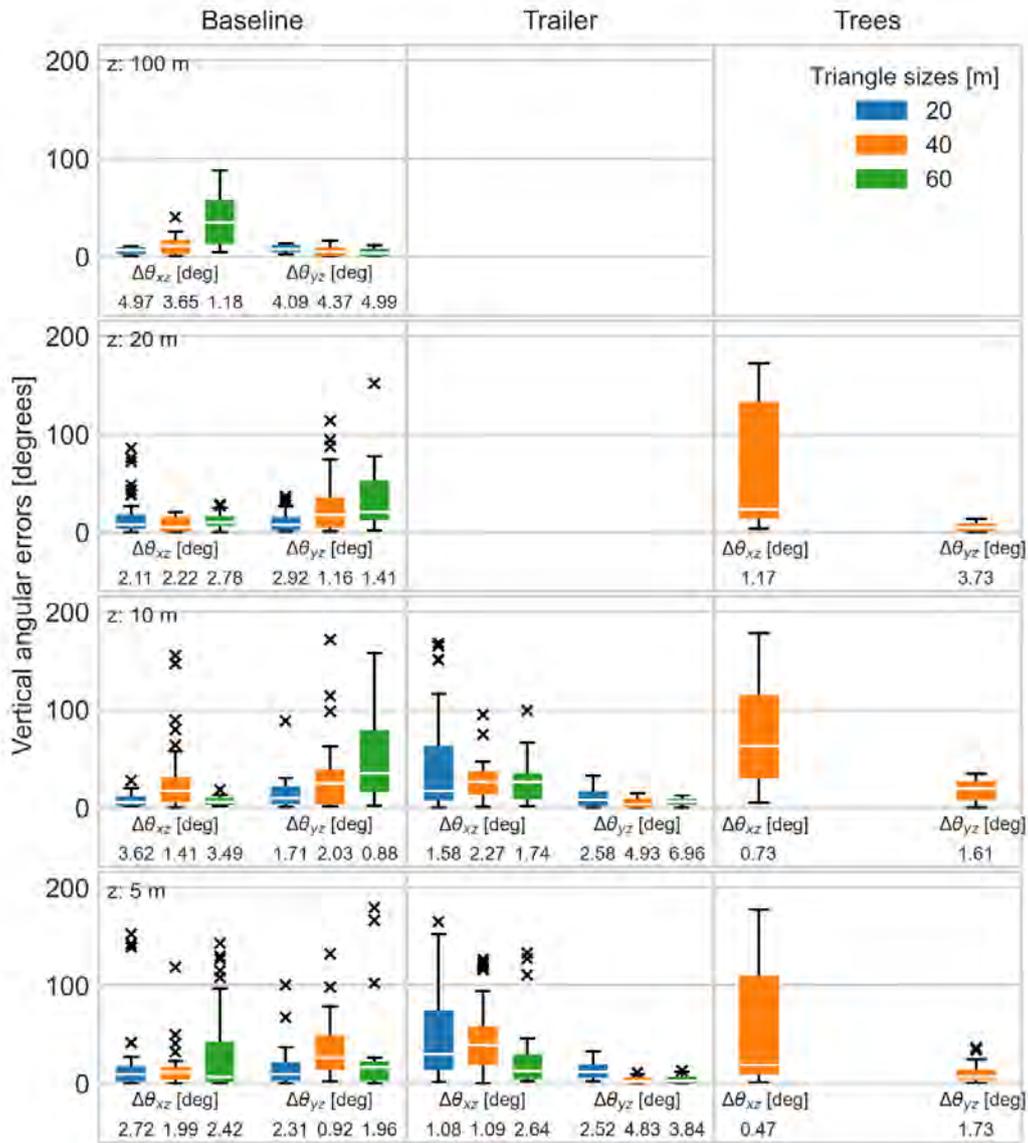
Figure 23: Vertical wind angular errors overview – static

Overall conclusion on the effect of static obstacles

Despite the relative high measurement error of the ultrasonic wind sensor during low wind scenarios, the MPM performs well on the horizontal magnitude and angular accuracy. The vertical magnitude accuracy of the MPM is difficult to judge due to poor sensor accuracy in the vertical direction. It is not possible to use the reference drone as ground truth in the vertical direction. Nonetheless, the MPM performs well given the average vertical magnitude, while lacking in modelling instantaneous changes. In contrast, the MPM performs exceptionally well on the vertical angular accuracy at high average wind speeds. The effect of obstacles on the error of the four independent variables are as follows:

- The effect of obstacles on the horizontal magnitude error seems negligible.
- The effect of obstacles on the vertical magnitude error seems negligible but somewhat inconclusive.
- The effect of trees on the horizontal angular error shows an increase in error, which is likely due to a decrease in wind speed by the obstacle-induced wind distortion.

- The effect of trees on the θ_{xz}-plane shows a significant increase in error, while the θ_{yz}-plane error is highly accurate. This may be due to respectively a decrease and increase in average wind speed on the respective plane and, therefore, random measurement error.

2.4.2.3 Research question 2: Effect of drone motion

This section will answer RQ2: How is accuracy affected by the motion of the drone? To answer this question, the static baseline scenario will be compared to the dynamic baseline scenario. The contour plots of the dynamic scenarios show dissimilarity between the wind direction of the static reference drone and the estimations of the MPM. Figure 24 shows such contour plot of the dynamic baseline scenario (triangle size 40 m, altitude 20 m) at three different timeframes, where the black arrows represent the MPM estimations, the blue arrow the reference drone measurements and the red arrows the measurement drone measurements. The green gradient indicates the confidence level of the wind field estimations. Given the MPM output matches the measurement drones input, the dissimilarity in wind direction between the reference and measurement drones suggests a measurement error.
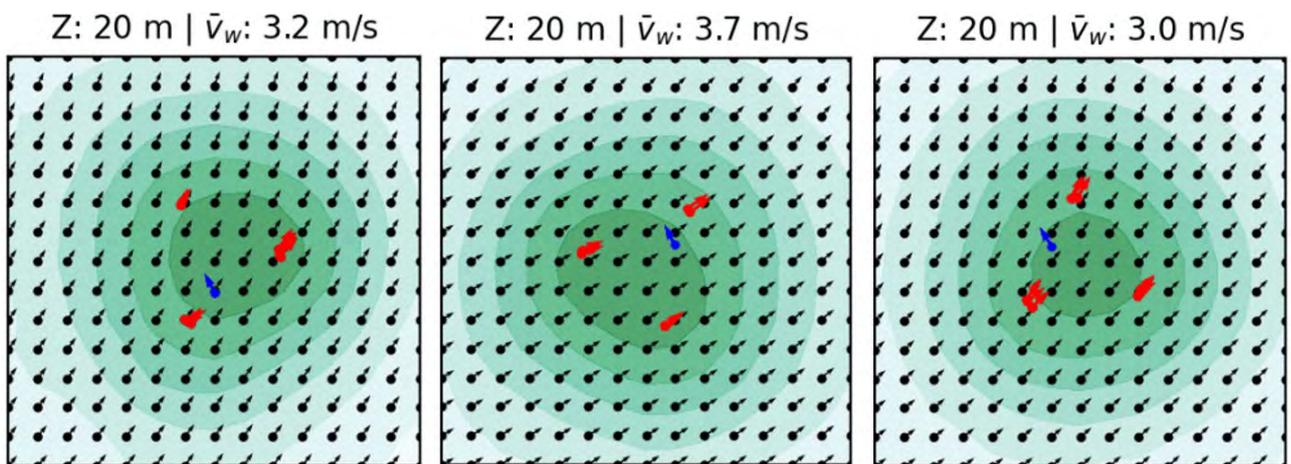
Figure 24: Contour plot of perceived measurement errors during dynamic scenarios
(red arrows: measurement drones, blue arrow: reference drone, black arrows: MPM estimates)

Plotting the horizontal wind magnitude and direction on ECEF-frame over the drone shows that the magnitude and direction follow a sinusoidal trend with the course; Figure 25. Wind is stochastic, and therefore, a clear sinusoidal trend is not representative of true wind states. Even though the drone motion is corrected for, the sinusoidal trend shows that the sensor measurements are incorrect. Correspondence with the wind sensor manufacturer Anemoment suggested that the motions of the drones are causing local turbulence around the TriSonica Mini. Nichols et al. (2017) investigated sources of error in inertial wind measurements from drones. They concluded that errors in aircraft state estimations (translation and rotation) have a great impact on the estimation of wind states. This aligns with the results shown in Figure 24, given the clear correlation between estimated wind magnitude and the drone course. Therefore, the dynamic scenarios of the METSIS experiment are unusable, and the effect of motion on the MPM accuracy remains inconclusive. A better solution for dynamic UAV-based wind measurements is required.
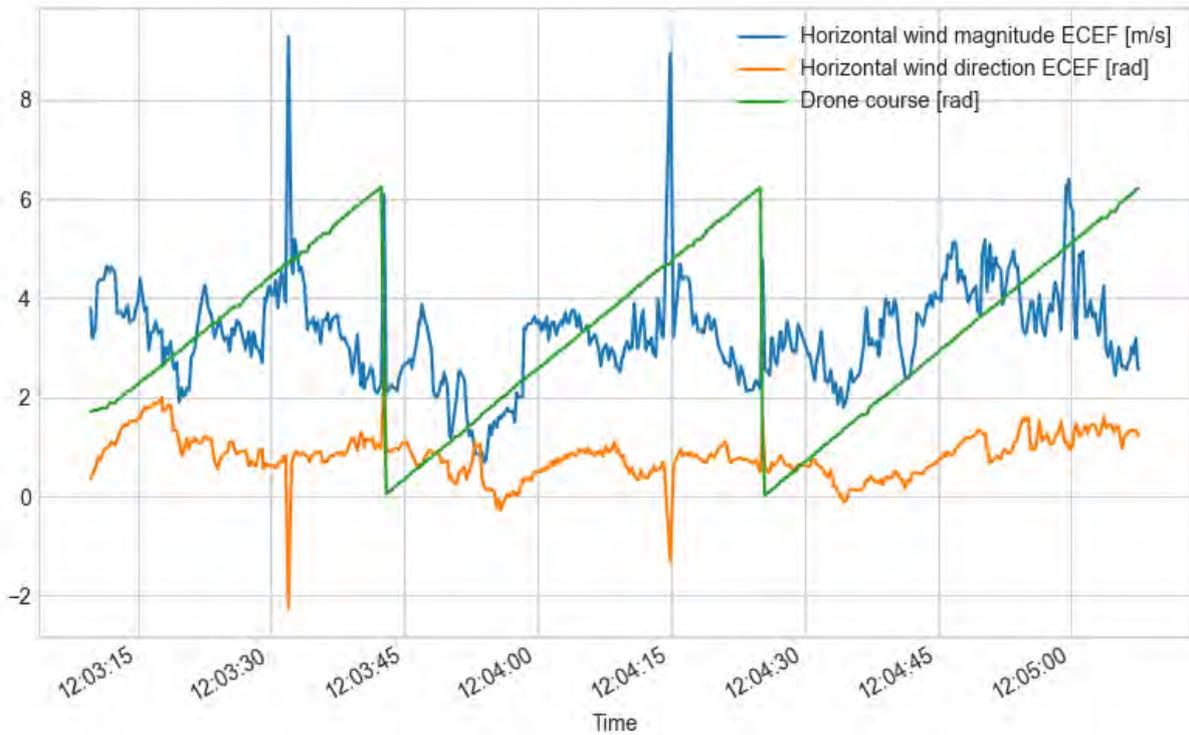
Figure 25: Line graph of the horizontal wind magnitude and direction with a clear sinusoidal trend given the drone course during dynamic scenarios

2.4.2.4   Research question 3: Effect of measurement density

This section will provide an answer to RQ3: How does the number of drones (i.e., measurement density) affect the accuracy of the wind field? To answer this question, only the static baseline scenario will be considered. By artificially deleting a measurement drone from the measurement data, the resulting accuracy of horizontal wind speed and direction will be compared to the accuracy depicted in Section 2.4.2.2.
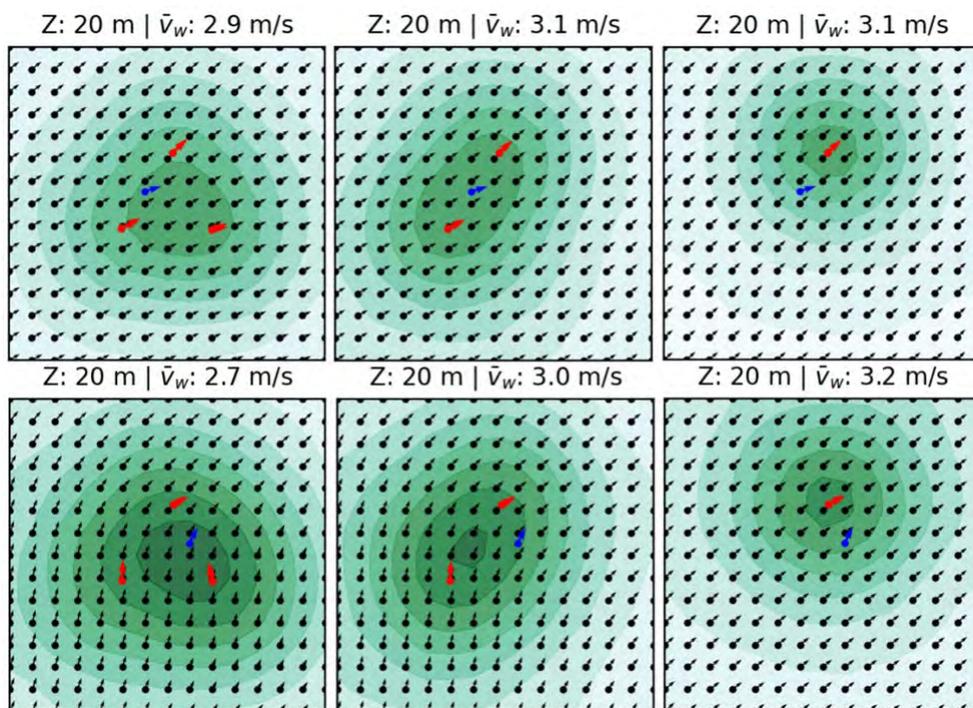
Figure 26: Contour plot (XY-plane, 20 metre altitude) comparison of drone density effect on accuracy

Figure 26 shows the contour plots of the baseline scenario with triangle size of 40 metres and altitude of 20 metres. The columns follow a sequential decrease in measurement drones at equal timeframes, while the rows represent two different reference drone locations. The green gradient describes the confidence level, where a darker green signifies a high level of confidence. Only a slight decrease in accuracy is perceived. Given Figure 25, at least two measurement drones are required at different locations for the MPM to be able to perceive changes in wind direction and speed.

Figure 27 compares the horizontal magnitude (left) and angular (right) errors for the entire baseline scenario by artificially deleting one and two drones. The reduced drone density can be compared against the original data with three measurement drones. Columns depict the different triangle sizes, and boxplot groups depict the number of measurement drones. No notable change in the wind magnitude and angular error is perceived. It is clear that the average wind velocity during the experiment day was low. At higher speeds, more drones could be necessary. However, a slight decrease in both magnitude and angular error is noticeable with a singular measurement drone. The boxplots and contour plots indicate there is a dependency on the number of drones. At the minimum, two measurement drones are required to have a more accurate depiction of alternations in wind direction. Nonetheless, the experiment took place on a single with a constant south-westerly wind. With more random wind, the decreasing number of drones could have a more significant impact. The effect of drone density on the MPM accuracy is not fully conclusive and requires more experimentation, but it shows promising results.
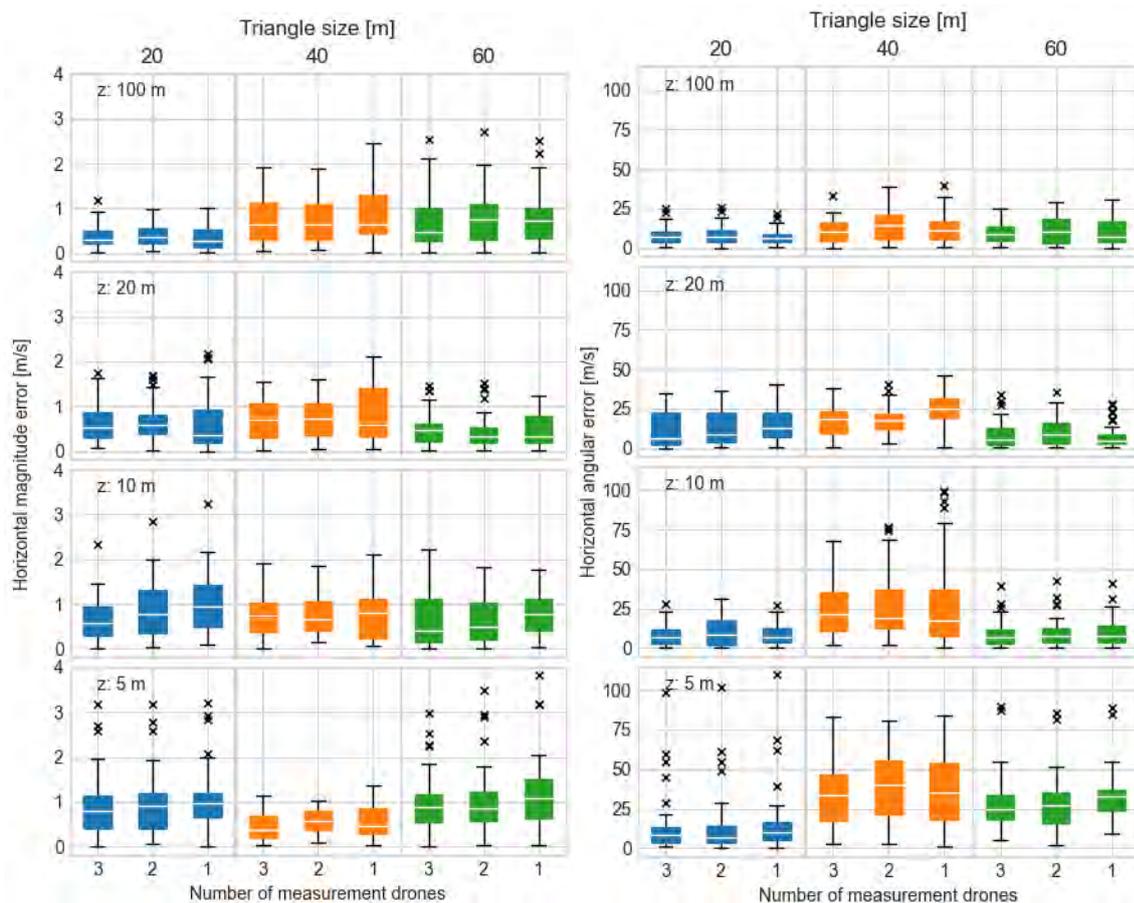
Figure 27: Comparison of horizontal magnitude (left) and angular (right) errors with decreasing drone density

2.4.2.5 Research question 4: Effect of measurement errors

RQ4, to what extent is the Meteo-Particle Model resilient to wind measurement errors by drones in the sensor network, will be answered by artificially adding Gaussian noise to the w_x, w_y, w_z, and course measurements of all measurement drones. This section only considers the entire static baseline scenario. The probabilistic rejection mechanism of the MPM (Section 2.1.2) is tested given the probability density function of Equation (19), by adding two strengths of Gaussian noise to all measurement drones (see Table 8) with respectively a standard deviation of 0.5 m/s and 1 m/s for the wind measurements, and 5 degrees and 10 degrees to the course measurements.

Table 8: Overview of the artificial Gaussian noise levels to wind and course measurements

	Low noise		High noise	
Measurement variable	w_x, w_y, w_z [m/s]	Course [deg]	w_x, w_y, w_z [m/s]	Course [deg]
Standard deviation σ	0.5	5	1.0	10
Mean μ	0	0	0	0
% of $\bar{v}_w$ (= 3.8 m/s)	13.1 %	-	26.2%	-

Figure 28 depicts the horizontal magnitude (left) and angular (right) error with an increase in Gaussian noise. There is no noticeable variation in error, even at the highest level of Gaussian noise. This indicates that the resiliency of the MPM performs exceptionally well given the relatively high noise on the sensor measurements. There seems to be no immediate need to modify the probabilistic rejection control parameter. However, the effect during increased wind velocities still has to be examined.
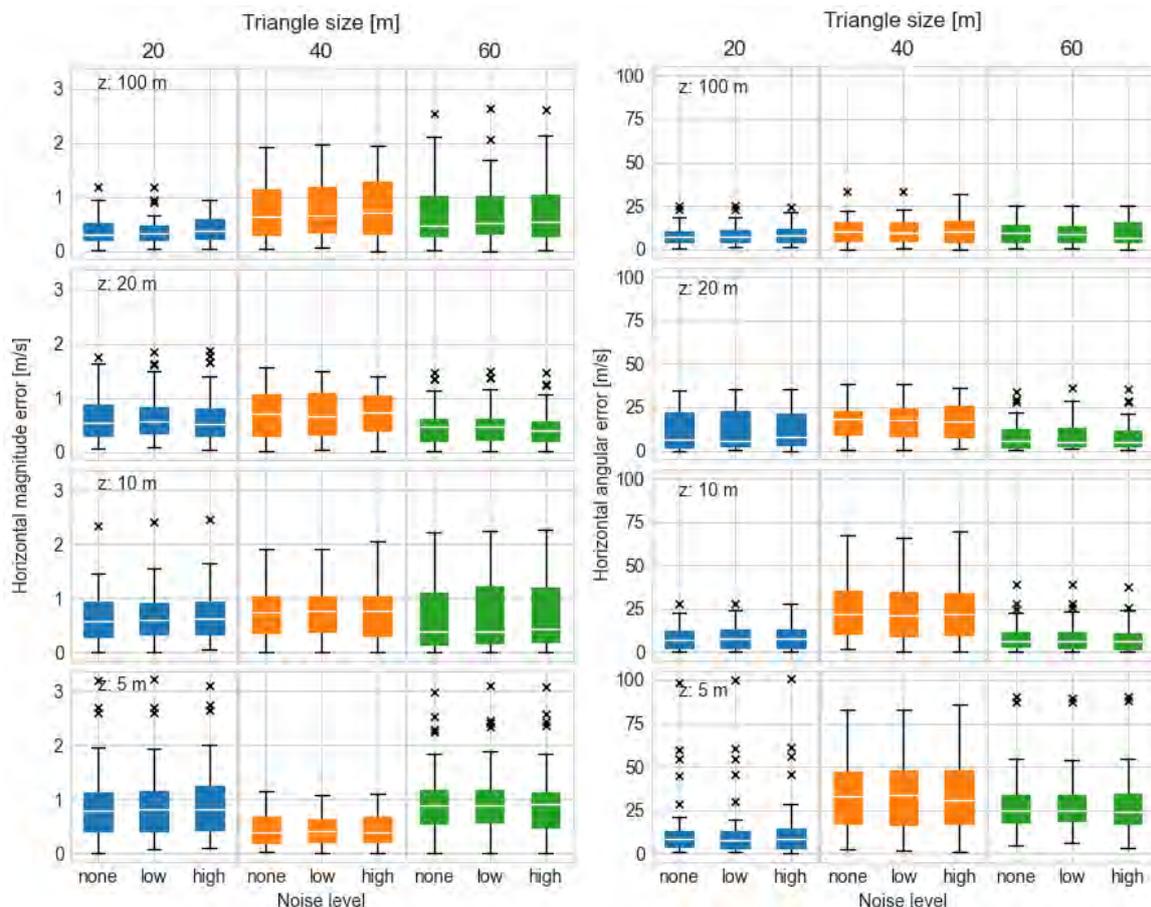

Figure 28: Comparison of horizontal magnitude (left) and angular (right) errors with artificially added Gaussian noise (none: no artificial noise, low: σ = 0.5 m/s & 5°, high: σ = 1.0 m/s & 10°)

2.4.2.6 Research question 5: Usage of the data in a U-space system

This sub-section describes how the real-time wind field data provided by NLR was processed and displayed on the AirHub Drone Operations Center (DOC) platform.

<u>Input processing</u>

Airhub received live 3D wind field data in JSON format from the METSIS ground station operated by NLR. Data was communicated using the HTTP POST method every 30 seconds. This incoming data was converted to GeoJSON for easier usage in the AirHub Drone Operations Center frontend. These results were cached in the backend until a new update was received from NLR. The DOC frontend requested the cached data and showed the GeoJSON in a vector field for visualization. Hereby some filter options were added to filter the wind based on the altitude of the measurement and the certainty of an observation.

<u>Human-Machine Interface (HMI) Design</u>

The AirHub DOC is a web-based application for planning, executing and logging drone operations. Drone flights can be performed remotely from the DOC through a real-time connection to the drone. For the METSIS project, AirHub plotted hyperlocal weather data in the live airspace UTM view of the DOC; see Figure 29. For drone operators it is important to have all relevant information available and directly visible for the flight planning and execution.

The following HMI elements have been ddeveloped for the project:

- Realtime display of the hyperlocal weather datasets on the live airspace map: On the airspace map in the DOC in which the drone operator sees all airspace restrictions, NOTAMS and obstacles, for his flight planning and execution, he/she now also has insight into the hyperlocal weather. This Hyperlocal weather is plotted on the map using wind arrows. This gives direct visible insight into the direction, magnitude, altitude of the wind. Moreover, wind is implemented as a visual layer on top of the airspace.
- Wind barb opacity interval slider: For a drone operator it is important to switch data information layers on and off quickly and easily, and in some cases to make it transparent so that he always retains a good overview. That is why we have built the opacity interface slider into the interface, so that the opacity can be adjusted to the wishes of the drone operator. This makes it possible to plot the wind without obstructing other parts of the live airspace UTM view of the DOC.
- Confidence interval slider: The certainty of the data is also an important factor for the planning and execution of a drone flight, for that reason we have also added the certainty interval slider for the hyperlocal wind. This gives the drone operator the freedom to decide for themselves the minimum confidence the wind data that is displayed on the DOC should have given the type of operation that is being performed.
- Wind altitude interval slider: A drone flies at different heights during an operation, so it is also important that the drone operator has a 3d image of the wind. We solved this in the HMI by adding an altitude slider – only wind at the selected altitude is displayed. This makes it easy to see what the data shows at different heights.

Sliders for arrow opacity,
wind data confidence and wind altitude

Wind speed
and direction

Detailed wind info
at selected location

Airspace view
with live UTM data

Filters
(wind/airspace etc.)
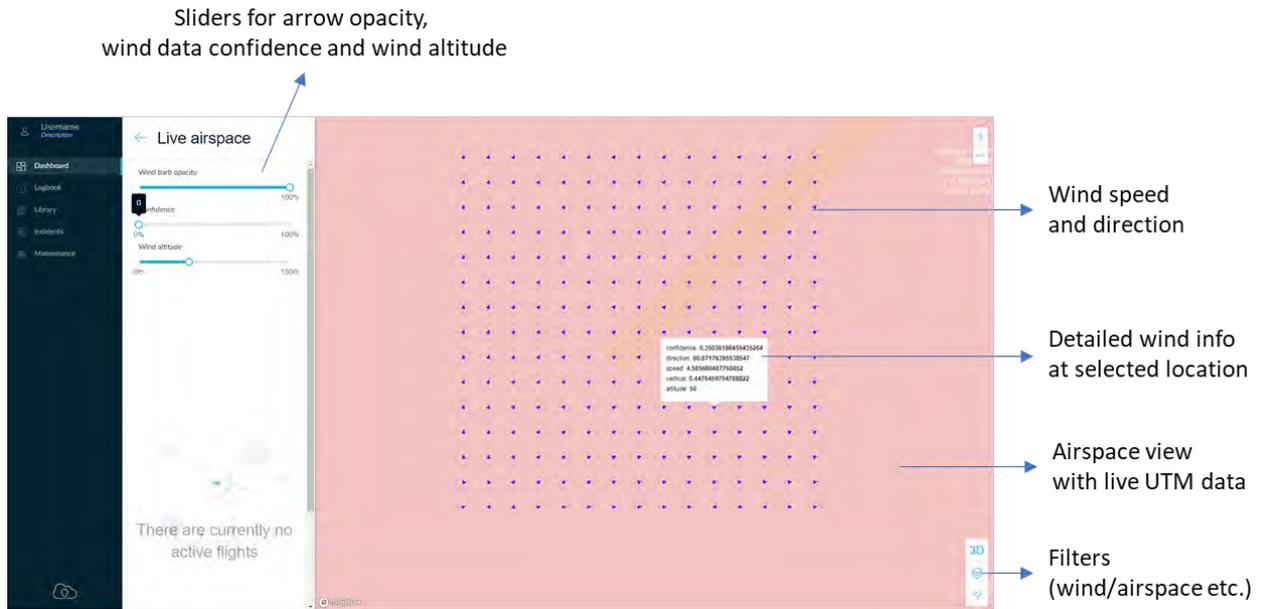
a) Real-time wind data collected during the experiment
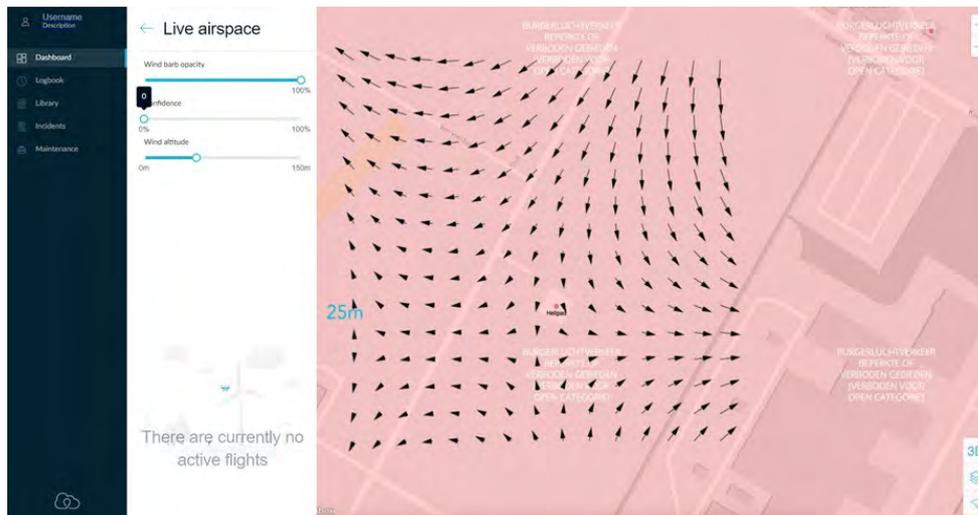
b) Simulated test wind data for illustrative purposes

Figure 29: AirHub Drone Operations Center (DOC) with real-time display of hyperlocal wind.

Experimental Evaluation

The above described method for communicating real-time wind data from the METSIS ground station to the AirHub DOC worked without any issues during the experiment, and new data was received every 30 seconds with negligible latency. To further improve the NLR-Airhub data communication procedure, it is recommended to investigate the use of web-sockets as an alternative to the HTTP POST used currently as web-sockets can achieve higher data throughputs. In addition, the new DOC hyperlocal wind HMI developed for this project also functioned flawlessly during the experiment.

3 Conclusions, next steps and lessons learned

3.1 Conclusions

The METeo Sensors In the Sky (METSIS) project tested the use of drones as an aerial sensor network for low-altitude hyperlocal wind nowcasting. The concept aims to provide accurate and low-cost wind nowcasts for drones using data collected by drones themselves, and thereby contribute to the U-space weather information service. A proof-of-concept flight-test experiment was performed at the NLR Drone Center using four drones to determine the feasibility of the METSIS concept at low altitudes over the course of a single day. In the current embodiment of the METSIS concept, ultrasonic anemometers were mounted to each drone to measure local winds. Wind fields estimated during the flight-tests were published in real-time to the AirHub Drone Operations Center – a U-space Service Provider – to demonstrate the communication of this data to real end-users.

This project resulted in the following main technical achievements:

- Wind tunnel testing of wind sensor: the accuracy of the ultrasonic wind sensor used in this project was measured in the NLR Anechoic Wind Tunnel for various wind tunnel speeds, angles of attack, and for two drone-propeller speeds.
- Meteo Particle Model extension: The MPM, which is used to estimate wind fields using drone observations, was extended to 3-dimensions, i.e., the vertical dimension was added to the MPM.
- Development of the METSIS ground station: the ground station aggregates the data from all the drones (and wind sensors), uses the MPM to estimate wind fields and logs all data.
- Real-time communication of wind data to a U-space Service Provider (USSP): The ground station also transmitted the MPM wind estimates in real-time to the AirHub Drone Operations Center. The data can also be communicated to other USSPs using the same approach.
- Drone-sensor configuration: four quadcopter drones were modified to mount the wind sensors onto the drones. This included modifications to the drone power supply and telemetry systems.
- Proof-of-concept flight-test experiment: A full day flight-test experiment using four drones was performed to study effects of obstacle-induced wind distortion, drone motion, measurement density, and measurement errors on the accuracy of the METSIS wind nowcasting system.

Based on the data collected during the flight-tests, the following main conclusions can be drawn:

- The flight-tests indicated that the METSIS concept is feasible in practice, i.e., that it is indeed possible to use drones as a weather sensor network for hyperlocal, low-altitude and real-time wind field estimations for U-space applications.
- When comparing the results of the experiment to the World Meteorology Organization (WMO) requirements for anemometers, the Meteo-Particle Model (MPM) showed satisfactory performance, especially during high wind speed scenarios. Therefore the MPM, which was originally developed for high altitude wind estimations for commercial aircraft, is considered suitable for low-altitude drone operations after the minor modifications made in this project.
- Answers to the main research questions of the METSIS project:

- o Effect of obstacles: Static obstacles had a minor effect on overall accuracy at the distances at which drones are expected to operate from obstacles. Obstacles had a greater impact on wind direction accuracy than on wind speed accuracy.
- o Effect of drone motion: given the low wind speeds during the experiment day, propeller induced flow had a strong negative effect on the measurements taken by the ultrasonic wind sensor during dynamic/motion scenarios. As such data collected from the current experiment could not be used to study the effect of motion on accuracy. This is an important topic to reconsider in future research.
- o Effect of number of drones/measurement density: The METSIS wind nowcasting system will only be able to model changes in wind direction if such wind direction changes are measured by one of the drones involved in the METSIS network. For the wind conditions observed during the experiment day, the results indicate that a minimum of two drones are needed for the MPM to accurately model changes in wind direction.
- o Effect of measurement error: No significant change in accuracy occurred when two different Gaussian noise models (with a standard deviation of 10% and 25% of the average wind speed during the experiment day) were artificially added to measured wind data. This indicates that the MPM's probabilistic rejection method can overcome some degree of random measurement errors. The effect of bias errors has not been considered here.
- o Communication of hyperlocal wind data to U-space Service Providers (USSPs): Wind data was communicated to the AirHub Drone Operations Center (DOC) in JSON format using the HTTP POST. This method proved to be a reliable means to communicate wind data to USSPs in real-time.

Because of the promising results obtained from the flight-tests, it is highly recommended to continue this line of research as the implementation of the METSIS concept on a larger scale could result in a viable system for hyperlocal wind nowcasts via the U-space weather information service. To this end, the following main recommendations are made to further develop this concept towards practical implementation:

- Repeat the experiment over multiple experiment days and consider more experiment conditions: The current experiment was performed over the course of a single day during which the wind was fairly homogenous. Therefore, it is recommended to repeat the experiment over the course of several days and with more obstacles to assess the concept for a variety of wind conditions, and thereby arrive at more conclusive answers to the research questions considered here.
- Reduce the effect of propeller induced flow over the wind sensor on accuracy: In this study, the effect of drone motion on accuracy could not be quantified because of the uneven propeller induced follow over the wind sensors during dynamic scenarios. It is recommended to research methods to deal with this so that accuracy during dynamic scenarios can be properly investigated. One option is to mount the sensor to the side of the drone instead on top of it as designed. Another option is to use the recent method proposed by Thielicke et al. (2021) to take into account propeller induced downwash on wind estimates based on the mean throttle value.
- Increase the scalability of the method: The current implementation of METSIS makes of direct wind measurements using ultrasonic wind sensors. To increase the scalability of the

METSIS concept, it is recommended to investigate indirect wind measurement techniques that do not make use of ultrasonic sensors. An example of this would be to infer wind speed and direction indirectly using ground speed and air speed measurements. This would require additional pressure sensors, but these are much cheaper than ultrasonic wind sensors (factor 10 cheaper). A downside of this approach compared to using ultrasonic sensors is that vertical winds cannot be measured – however this limitation may not be critical for most use cases. If the wind sensor can be removed from the METSIS concept, the previous bullet point does not need to be considered for future research.

- Online optimization of MPM parameters: The accuracy of the method is dependent on the settings of the MPM. For this project static settings were used throughout the experiment. It is worth investigating if dynamically varying the MPM parameters during flight can reduce the error between MPM estimates and the true wind states. This could be achieved by implementation a stochastic optimization method such as Particle Swarm Optimization (PSO) (Kennedy, J., Eberhart, R., 1995). Regardless of the optimization method used, the main challenges with this approach lies in defining a suitable objective function, or perhaps multiple objective functions, and speed of the optimization.

- Data communication to USSPs: Future implementations should transmit wind data to USSPs in the GeoJSON data format as this is more widely used for weather data, and use web-sockets for data transmission as this is more scalable than the HTTP Post method considered here.

- Applications of hyper-local wind: The current research focused on measuring and communicating wind data. A logical follow up would to be demonstrate the use of this information for optimizing drone operations, including methods that drone operators can use to compute wind optimized routes to increase drone range/battery life. This would help to illustrate the utility of the METSIS concept in every-day drone operations.

- Explore the viability of the METSIS concept to other weather parameters such as temperature and air pressure.

3.2   Next steps

The following dissemination activities are planned in the near future:

1. Participation in the Engage TC 3 (MET) virtual workshop in September 2021 as a panelist
2. Scientific conference paper (most likely for SID 2021) about the METSIS concept, experiment results and recommendations for future research in this topic.

The following actions are recommended to further develop project outcomes:

1. In order to bring the METSIS concept closer to real-world implementation, the next step would be to initiate a larger-scale research project that focuses on the technical recommendations mentioned in Section 3.1. The goal of such a large-scale project should be to improve the accuracy, the scalability and usability of the METSIS concept, as well as test the concept for a wider range of scenarios than what was considered in the present project, including scenarios in urban settings. In addition to NLR and AirHub, the consortium for such a project should involve a university, a drone manufacturer and a meteorological research institute/industry. Ideally, additional U-space service providers can also be involved to speed

up the eventual commercialization of the METSIS technology. The most suitable avenue for financing this larger-scale project would be the upcoming SESAR 3 calls expected in 2022 – especially since the project aims to support the development of the U-space weather information service.

2. In parallel to the preparations for the larger-scale project, it would also be ideal to use the infrastructure developed for the METSIS project to initiate smaller-scale internal research projects to investigate specific and limited improvements to the METSIS concept. An example of such a project could be to investigate the viability of indirect wind measurements for drones using airspeed and ground speed measurements. Any improvements resulting from such smaller-scale projects could then be validated in detail through the larger-scale project mentioned above.

3.3   Lessons learned

The following lessons have been learned with respect to management aspects:

- As always, the cooperation between NLR and AirHub went smoothly during this project.
- COVID caused significant delays in procuring the materials needed for this project. For example, the drones were delivered three months after the initial order was placed. But such delays were mostly absorbed by the slack available in the original planning. This meant that several tasks had to be performed in parallel to complete the project on time. This proved to be tricky from a staff resource management perspective.
- A project advisory board consisting of experts from TU Delft and KNMI participated in this project. During the course of the project, four advisory board meetings were conducted. The advisory board members provided insightful advice that helped the project to stay on track.
- The 'light touch' approach of catalyst projects made it possible to devote almost all available resources towards the technical and dissemination outputs of this project. Very little effort was required to fulfil the administrative obligations of this project. Furthermore, Engage answered all administrative questions very quickly.
- It would be recommended to continue catalyst-type R&D projects in future SESAR KTNs. This approach makes it possible to take some technical risks without the complexity of a large project with many partners that can be difficult to coordinate. But on the other hand, it is very important to set achievable targets given the size of the project in order to be successful.

4 Dissemination

Table 9 lists the dissemination activities that have been completed and those that are planned in the future. Note that dissemination activities that are planned for the future have also been described in Section 3.2.

Table 9: Performed and planned dissemination activities

#	Date	Item	Link
1	July 2020	Press release on NLR website at the start of the project	[Click here]
2	December 2020	Poster at SESAR Innovation Days 2020 (incl. video presentation)	[Click here] (registration required)
3	January 2021	Project presentation at Engage Thematic Workshop #3 (MET integration in ATM)	[Click here]
4	July 2021	METSIS presentation at Amsterdam Drone Week Industry Update 2021	[Click here] (registration required)
5	July 2021	NLR METSIS video for YouTube and LinkedIn	[YouTube] and [LinkedIn]
6	July 2021	SESAR Newsletter	[Click here]
7	July 2021	News article on dronewatch.nl	[Click here]
8	July 2021	METSIS Final Technical Report	-
9	September 2021 (Planned)	Panel presentation at Engage Thematic Workshop (MET integration in ATM)	-
10	Planned	Conference paper (most likely SESAR Innovation Days)	-

5   References

5.1   Project outputs

Note, only the project outputs completed so far are listed below. In addition to these, the planned outputs are indicated in Table 9.

NLR Media Team Press Release (2020). *Kick-off METSIS Project – real-time weather information for drone operators.* https://www.nlr.org/news/kick-off-metsis-project-real-time-weather-information-for-drone-operators/

NLR Media Team YouTube Video (2021). *METeo Sensors In the Sky (METSIS) project.* https://www.youtube.com/watch?v=-OVcgA3-hRQ

NLR Media Team LinkedIn Post (2021). https://www.linkedin.com/posts/nlr_wind-nowcasts-for-drones-by-drones-activity-6818494329657532416-ViYW/

Sunil, E. (2020). *METSIS: METeo Sensors In the Sky, Investigating the use of drones as an aerial sensor network for low altitude hyper-local wind now-casting.* Poster at SESAR Innovation Days (SIDs) 2020. https://whova.com/portal/webapp/sesar1_202012/exhibitors/113375/

Sunil, E. (2021). *METSIS: METeo Sensors In the Sky.* Project Presentation at Engage Thematic Workshop on MET Integration in ATM January 2021. https://engagektn.com/thematic-challenges/

Sunil, E. (2021), *METSIS: METeo Sensors In the Sky.* Presentation at Amsterdam Drone Week Industry Update 2021. https://matchmaking.grip.events/adw/app/home

Sunil, E., Koerse, R., van Selling, S., van Doorn, J.W., Brinkman, T. (2021). *METSIS Final Technical Report.* SESAR Engage Catalyst Project

5.2   Other

Barbieri et al. (2019). *Intercomparison of Small Unmanned Aircraft System (sUAS) Measurements for Atmospheric Science during the LAPSE-RATE Campaign.* Sensors 2019, 19(9), 219. https://doi.org/10.3390/s19092179

Botchkarev, A. (2018). *Performance Metrics (Error Measures) in Machine Learning Regression, Forecasting and Prognostics: Properties and Typology.* https://doi.org/10.28945/4184

Brouwer, H.H. (1997). *Anechoic wind tunnels.* Royal Netherlands Aerospace Centre. https://reports.nlr.nl/xmlui/bitstream/handle/10921/1297/TP-1997-517.pdf

Chai, T., Draxler, R. R. (2014). *Root mean square error (RMSE) or mean absolute error (MAE)? - Arguments against avoiding RMSE in the literature.* Geosci. Model Dev., 7, 1247–1250. https://doi.org/10.5194/gmd-7-1247-2014

CORUS (2019), *Concept of Operations for U-space Ed 01.01.03*
https://www.sesarju.eu/projects/corus

Dahiru, T. (2008). *P-value, a true test of statistical significance? A cautionary note*. Ann Ib Postgrad Med. 2008 Jun; 6(1): 21-26.
https://www.ncbi.nlm.nih.gov/pmc/articles/PMC4111019/

Dowdy, S., Wearden, S., Chilko, D. (2004). *Statistics for Research*. Hoboken, NJ: John Wiley & Sons.

Frost, J. (2021). *Understanding Interaction Effects in Statistics*. Statistics by Jim.
https://statisticsbyjim.com/regression/interaction-effects/

Hashem, P.M. (2015). *Time Series and Panel Data Econometrics.* New York: Oxford University Press. pp. 67-72.

Hyndman, R.J. (2009). *Moving averages*. Retrieved from:
https://robjhyndman.com/papers/movingaverage.pdf

International Organization for Standardization. (1994). *Accuracy (trueness and precision) of measurement methods and results - Part 1: General principles and definition* (ISO Standard No. 5725). https://www.iso.org/obp/ui/#iso:std:iso:5725:-1:en

Kardasz, P., Doskocz, J. (2016). Drones and Possibilities of their Using. Journal of Civil & Environmental Engineering 6(3). https://doi.org/10.4172/2165-784X.1000233

Kastner-Klein, P., Fedorovich, E., Rotach, M.W. (2001). *A wind tunnel study of organised and turbulent air motions in urban street canyons*. Journal of Wind Engineering and Industral Aerodynamics. https://doi.org/10.1016/S0167-6105(01)00074-5

Kennedy, J., Eberhart, R. (1995). *Particle swarm optimization*. Proceedings of IEEE International Conference on Neural Networks, pp. 1942-1948.
https://doi.org/10.1109/ICNN.1995.488968

Kenton, W. (2020). *What is a Probability Density Function (PDF)?* Investopedia.
https://www.investopedia.com/terms/p/pdf.asp

Khoufi, I., Laouiti, A., Adjih, C., Hadded, M. (2021). *UAVs Trajectory Optimization for Data Pick Up and Delivery with Time Window*. Drones 2021, 5(2), 27.
https://doi.org/10.3390/drones5020027

Kick-off METSIS Project – real-time weather information for drone operators. (2020). Royal Netherlands Aerospace Centre. https://www.nlr.org/news/kick-off-metsis-project-real-time-weather-information-for-drone-operators/

Kroese, D.P., Brereton, T., Taimre, T., Botev, Z.I. (2014). *Why the Monte Carlo method is so important today*. WIREs Comput Stat 2014, 6:386-392. https://doi.org/10.1002/wics.1314

Langelaan, J.W., Alley, N., & Neidhoefer, J. (2011). *Wind Field Estimation for Small Unmanned Aerial Vehicles*. Journal of Guidance, Control and Dynamics, Vol. 34, No. 4, 2011. https://doi.org/10.2514/1.52532

McClave, J.T., Benson, P.G., Sincich, T. (2008). *Statistiek voor Techniek en ICT*. Pearson Education Benelux.

Nichols, T., Argrow, B., Kingston, D. (2017). *Error Sensitivity Analysis of Small UAS Wind Sensing Systems.* https://doi.org/10.2514/6.2017-0647

Pachter, M., Ceccarelli, N., Chandler, P. (2012). *Estimating MAV's Heading and the Wind Speed and Direction Using GPS, Inertial, and Air Speed Measurements.* AIAA Guidance, Navigation and Control Conference and Exhibit. https://doi.org/10.2514/6.2008-6311

Pittelkau, M.E. (2003). *Rotation Vector in Attitude Estimation*. Journal of Guidance, Control, and Dynamics. Vol. 26, No. 6. https://doi.org/10.2514/2.6929

Python Software Foundation: Press Release. (2003). Python Software Foundation. https://www.python.org/psf/press-release/pr20030213/

Qiao, T., Sambo, Y.A., Imran, M.A., Ahmad, W. (2020). *Drone Trajectory Optimization using Genetic Algorithm with Prioritized Base Stations.* IEEE 25th International Workshop on Computer Aided Modeling and Design of Communication Links and Networks (CAMAD). https://doi.org/10.1109/CAMAD50429.2020.9209291

Rhudy, M., Larrabee, T., Chao, H., Gu, Y., & Napolitano, M. R. (2013). *UAV Attitude, Heading, and Wind Estimation Using GPS/INS and an Air Data System.* http://dx.doi.org/10.2514/6.2013-5201

Sasaki, K., Inoue, M., Shimura, T., Iguchi, M. (2021). *In Situ, Rotor-Based Drone Measurement of Wind Vector and Aerosol Concentration in Volcanic Areas.* Atmosphere 12, No. 3: 376. https://doi.org/10.3390/atmos12030376

Scikit-learn developers. (2020). *Ordinary least squares Linear Regression.* *https://scikit-learn.org/stable/modules/generated/sklearn.linear_model.LinearRegression*

SESAR (2018), *European ATM Master Plan: Roadmap for the safe integration of drones into all classes of the airspace.* https://www.sesarju.eu/sites/default/files/documents/reports/European%20ATM%20Master%20Plan%20Drone%20roadmap.pdf

Stone, D.C. (1995). *Application of median filtering to noisy data.* Canadian Journal of Chemistry. https://doi.org/10.1139/v95-195

Sun, J., Vû, H., Ellerbroek, J., & Hoekstra, J.M. (2018). *Weather field reconstruction using aircraft surveillance data and a novel meteo-particle model*. PloS ONE 13(10): https://doi.org/10.1371/journal.pone.0205029

Supporting Safe and Secure Drone Operations in Europe. (2020). SESAR Joint Undertaking. doi: 10.2829/55322

Taylor, J.R. (1997). *An introduction to Error Analysis*. Sausalito, CA: University Science Books.

Thielicke, W., Hübert, W., Müller, U., Eggert, M. & Wilhelm, P. (2021). *Towards accurate and practical drone-based wind measurements with an ultrasonic anemometer.* AMT, 14, 1303-1318. https://doi.org/10.5194/amt-14-1303-2021

Van Bussel, G.J.W. (2008). *Wind Resource – Wind obstacles/Wind shade*. TU Delft. http://mstudioblackboard.tudelft.nl/duwind/Wind%20energy%20online%20reader/

Venter, Z.S., Brousse, O., Esau, I., Meier, F. (2020). *Hyperlocal mapping of urban air temperature using remote sensing and crowdsourced weather data*. https://doi.org/10.1016/j.rse.2020.111791

Wang, B.H., Wang, D.B., Ali, Z.A., Ting, B.T., Wang, H. (2019). *An overview of various kinds of wind effects on unmanned aerial vehicles.* Measurement and Control. Vol. 52; 7-8. https://doi.org/10.1177%2F0020294019847688

Wei, G., Ma L., Wang Z., Ding D., Hu J. (2015). *Filtering and Control for Unreliable Communication*. Discrete Dynamics in Nature and Society, vol. 2015, Article ID 278018. https://doi.org/10.1155/2015/278018

Wen, Y., Tsai, Y., Wu, D., Chen, P. (2013). *The Impact of Outliers on Net-Benefit Regression Model in Cost-Effectiveness Analysis.* PLoS One, 2013; 8(6). https://dx.doi.org/10.1371%2Fjournal.pone.0065930

World Meteorological Organization (2009). *Nowcast*. Eumetcal. Archived from the original on June 5, 2016. http://www.eumetcal.org/euromet/glossary/nowcast.htm

World Meteorological Organization. (2014). *Part I. Measurement of meteorological variables - Chapter 5: Measurement of surface wind*. Retrieved from: https://library.wmo.int/doc_num.php?explnum_id=3177

World Meteorological Organization. (2017). *Guidelines for Nowcasting Techniques.* Retrieved from: https://library.wmo.int/doc_num.php?explnum_id=3795

Xia, F., Liu, J., Nie, H., Fu, Y., Wan, L., Kong, X. (2019). *Random Walks: A review of Algorithms and Applications*. Transactions on Emerging Topics in Computational Intelligence. Vol. 4, No. 2. https://doi.org/10.1109/TETCI.2019.2952908

Zamboni, J. (2018). *What is the Meaning of Sample Size?* Sciencing. https://sciencing.com/meaning-sample-size-5988804.html

Zhang, Y., Wang, S., Ji, G. (2015). *A Comprehensive Survey on Particle Swarm Optimization Algorithm and Its Applications.* Artificial Intelligence and Its Applications 2015. https://doi.org/10.1155/2015/931256

6   Annex I: Acronyms

ADS	Air Data System
ADS-B	Automatic Dependent Surveillance-Broadcast
AOAP	Aerospace Operations division ATM and Airport
API	Application Programming Interface
ASL	Above Sea Level
ATM	Air Traffic Management
AUAS	Amsterdam University of Applied Sciences
CNS	Communication, Navigation and Surveillance
DGS	Drone Ground Station
DOC	(AirHub) Drone Operations Center
ECEF	Earth-Centered, Earth-Fixed
GNSS	Global Navigation Satellite System
GPS	Global Positioning System
GUI	Graphical User Interface
HMI	Human-Machine Interface
HTTP	Hypertext Transfer Protocol
IMU	Inertia Measurement Unit
INS	Inertial Navigation System
JSON	JavaScript Object Notation

KTN	Knowledge Transfer Network
LIDAR	Light Detection and Ranging
MAE	Mean Absolute Error
MAPE	Mean Absolute Percentage Error
METSIS	Meteo Sensors in the Sky
MPM	Meteo-Particle Model
NLR	Royal Netherlands Aerospace Centre
PSO	Particle Swarm Optimization
PUB/SUB	Publisher/Subscriber
RMSE	Root Mean Square Error
SESAR	Single European Sky ATM Research
SGS	Sensor Ground Station
TU Delft	Delft University of Technology
USSP	U-space Service Provider
WMO	World Meteorological Organization

7 Annex II: Glossary

Accuracy	When repeated measurements are accurate, the measurements are close to the true value of the quantity being measured and offers smaller measurement error. In contrast to error, accuracy is the degree of closeness to the exact value (International Organization for Standardization [ISO], 1994).
ADS-B	Automatic Dependent Surveillance-Broadcast (ADS-B) is a surveillance technology in which an aircraft determines its position via satellite navigation or other sensors and periodically broadcasts it, enabling it to be tracked (Sun, Vû, Ellerbroek, & Hoekstra, 2018).

Anechoic	Synonym for "non-reflective", meaning a space designed to completely absorb reflections of either sound or electromagnetic waves (Brouwer, 1997). In this project, an anechoic wind tunnel is used to reduce background noise during the sensor testing.
Anemometer	A synonym for wind sensor, a device used to measure wind speed and direction.
Control parameter	The idea of parameter control is to vary the model's parameters so that the algorithm of interest may achieve the best performance under certain circumstances.
Covariance (Cov)	Covariance is a measure of the joint variability of two random variables (Dowdy, Wearden, & Chilko, 2004).
Error	Experimental error is defined as the exact difference between an experimental value and the actual value (ISO, 1994).
Exponential (exp)	In mathematics, the most important exponential function is $y = e^x$, sometimes written $y = exp(x)$, in which e is the base of the natural system of logarithms (ln). Exponential functions are often used to represent real-world applications (Dowdy et al., 2004).
Hyper-local	Is defined as the geographical scale of weather field mapping of 10–30 meters spatial resolution (Venter et al., 2020).
Line of best fit	Also called a "trend line", which is a line that minimises the residual sum of squares between the observed targets in the dataset, and the targets predicted by the linear approximation (scikit-learn developers, 2020).
MAE	The Mean Absolute Error is a scoring rule that measures the average error for one specific observation (Chai & Draxler, 2014). A boxplot is a method to visualise the distribution of the measured MAE of multiple observations.
MAPE	The Mean Absolute Percentage Error is fundamentally similar to the MAE, except it offers an idea of the magnitude of the error in relation to the actual values (Botchkarev, 2018). Commonly, the results are multiplied by 100 to present the ratio as a percentage. Normalization by actuals is often referred to as percentage metrics.
Mean (μ)	Researchers use the mean to make statements about the centre of measurement data (Dowdy et al., 2004). The mean is the average of the sample or population that is being measured. The Greek letter μ (mu) is the symbol used for "mean".

Mode S	Mode S is a Secondary Surveillance Radar process that allows selective interrogation of aircraft according to the unique 24-bit address assigned to each aircraft (SKYbrary, 2018).
Monte Carlo	A Monte Carlo simulation is the modelling of random objects or processes by prediction of the probability of different outcomes (Kroese et al., 2014).
Nowcasting	Forecasting weather in real-time to a couple of hours using instantaneous weather data (World Meteorological Organization, 2009).
Particle	For this project, particles can be considered as the information medium that carry parameter values such as the location (x, y, z), wind speed and wind direction (Sun, Vû, Ellerbroek, & Hoekstra, 2018).
Precision	In contrast to accuracy, where a measurement can be said to be accurate if their value is close to the true value of the quantity being measured, precision determines whether the measured values are close to each other where the least amount of variation suggests a high precision (Dowdy et al., 2004).
Probability (P)	In an experiment, the probability is a value between (and including) zero and one which is the likelihood of that event occurring during the experiment (McClave, Benson, & Sincich, 2008). If $P(E)$ represents the probability of an event *E*, then: • $P(E) = 0$ if and only if *E* is an impossible event. • $P(E) = 1$ if and only if *E* is a certain event. • $0 \leq P(E) \leq 1$. Given the two events "A" and "B", $P(A) > P(B)$ if and only if event "A" is more likely to occur than event "B".
Python	Python is a programming language designed and developed by Guido van Rossum in the early 1990s, where the main characteristics of Python are readability and simplicity (Python Software Foundation, 2003).
Random walk	A random walk is defined as a random process in mathematical space. It can be used to analyse and simulate stochastic natural phenomenon, such as the chaotic nature of wind (Xia et al., 2019).
Residual	The residual of an observed value is the difference between the observed value and the estimated value of the measured quantity (Dowdy et al., 2004).

Sample size	Sample size refers to the number of individual samples or observations used in an experiment. A small sample size will yield unreliable results (Zamboni, 2018).
Set membership (∈)	Set membership is denoted by the symbol "∈". Writing "$x \in A$" means that x is an element of set A.
Sigma (Σ)	In general mathematics, uppercase Σ is used as an operator for summation.
Standard deviation (σ)	The standard deviation measures the variation of the values of a variable around its mean value (Dowdy et al., 2004). Put simply, the standard deviation is the average distance from the mean value of all values in a dataset.
Stochastic	Stochastic refers to the property of being well described by a random probability distribution. In probability theory, the formal concept of a stochastic process is also referred to as a random process (Xia et al., 2019).
Variance (σ^2)	The term variance refers to a statistical measurement of the spread between numbers in a data set. More specifically, variance measures how far each number in the set is from the mean (Dowdy et al., 2004). The square root of the variance is the standard deviation (σ).
Wind distortion	Wind distortion means the deformation/turbulence in wind flow (speed and direction) induced by an obstacle (Van Bussel, 2008).
Wind gradient	Is defined as a variation of wind speed or direction in the vertical direction (Langelaan et al., 2011).

8 Annex III: Experiment Plan Excerpt

Scenario 1 - baseline			
Start time:			
Parameters		**Pre-check**	
Position [lat, long]	[52.679967, 5.920998]	Wi-Fi:	
Triangle sizes [m]	[60, 40, 20]	Drone data:	
Altitudes [m]	[5, 10, 20, 100]	Sensor data:	
Motion [m/s]	[0, 3]		
Obstacle	None		
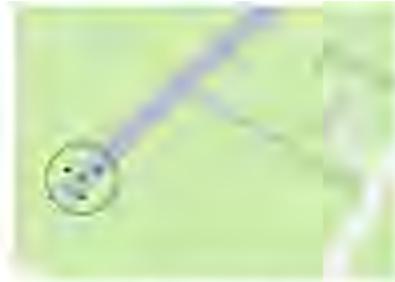
MissionPlan	Rotations	Combinations	Speed	✔	Notes	Post-check	
Test 1	2	Triangle size [60] : altitude [5]	0			Logs	
			3			Figures	
	2	Triangle size [60] : altitude [10]	0			Logs	
			3			Figures	
	2	Triangle size [60] : altitude [20]	0			Logs	
			3			Figures	
Test 2	3	Triangle size [40] : altitude [5]	0			Logs	
			3			Figures	
	3	Triangle size [40] : altitude [10]	0			Logs	
			3			Figures	
	3	Triangle size [40] : altitude [20]	0			Logs	
			3			Figures	
Test 3	5	Triangle size [20] : altitude [5]	0			Logs	
			3			Figures	
	5	Triangle size [20] : altitude [10]	0			Logs	
			3			Figures	
	5	Triangle size [20] : altitude [20]	0			Logs	
			3			Figures	
Test 4	2	Triangle size [60] : altitude [100]	0			Logs	
			3			Figures	
	3	Triangle size [40] : altitude [100]	0			Logs	
			3			Figures	
Test 5	5	Triangle size [20] : altitude [100]	0			Logs	
			3			Figures	

9   Annex IV: Experiment Results Per Scenario

Table 10: Overview of the METSIS experiment 3D magnitude and horizontal and vertical angular MAE

Scenario	Altitude [m]	Triangle [m]	Speed [m/s]	$\bar{v}_w$ [m/s]	MAE w_{mag} [m/s]	MAPE w_{mag} [%]	MAE θ_{hor} [deg]	MAE θ_{ver} [deg]
Scenario 1 (baseline)	5	20	0	3.57	0.8754	22.8	14.5	18.8
			3	2.86	0.7271	24.2	99.9	99.3
		40	0	2.28	0.4160	18.0	33.4	25.5
			3	3.14	0.5997	20.8	70.8	75.7
		60	0	3.30	0.9578	25.1	28.9	27.7
			3	3.33	0.5079	17.7	54.2	51.9
	10	20	0	3.98	0.6608	17.8	8.00	10.8
			3	3.14	0.5083	17.0	90.9	93.9
		40	0	2.50	0.7149	26.9	26.1	29.6
			3	3.70	1.1325	28.5	59.7	58.9
		60	0	3.58	0.7310	16.5	8.7	29.1
			3	3.01	0.6378	30.0	42.7	65.3
	20	20	0	3.64	0.6367	17.0	12.9	13.9
			3	3.05	0.4429	14.7	95.7	84.2
		40	0	2.64	0.7047	25.2	17.4	17.3
			3	3.20	0.4761	15.4	63.2	66.8
		60	0	3.11	0.4694	15.5	9.0	22.3
			3	3.64	0.7227	20.3	45.8	51.8
	100	20	0	6.40	0.3631	5.7	8.13	6.82
			3	5.00	0.6314	13.9	84.2	79.2
		40	0	5.66	0.7302	13.7	10.7	8.6
			3	5.21	0.5590	10.9	62.9	74.5
		60	0	5.12	0.6990	14.1	9.6	20.9
			3	5.10	0.9776	19.4	38.0	28.0
Average:			0	3.82	0.6632	18.2	15.6	19.3
			3	3.70	0.6603	19.4	67.3	69.1
Scenario 2 (trailer)	5	20	0	2.77	0.6803	23.8	14.2	30.5
			3	2.83	0.4465	13.8	100.9	94.5
		40	0	4.90	0.8058	18.7	10.2	25.0
			3	4.15	0.6670	17.7	69.7	48.9
		60	0	4.79	1.0677	24.2	19.8	14.0
			3	4.11	1.2075	36.7	41.7	31.2
	10	20	0	3.13	0.7317	23.8	15.0	27.0
			3	3.13	0.7670	23.2	93.4	94.8
		40	0	5.42	0.7397	14.4	12.6	16.5
			3	3.83	0.7350	19.3	68.1	51.7
		60	0	7.13	0.8780	13.0	5.6	17.2
			3	3.49	0.7978	24.8	45.1	50.3
Average:			0	4.69	0.8172	19.7	12.9	21.7
			3	3.59	0.7701	22.6	69.8	61.9
Scenario 3 (trees)	5	40	0	1.81	0.7120	46.5	15.0	33.3
			3	1.15	0.7591	46.6	61.4	74.5
	10	40	0	1.82	0.5635	38.4	23.6	47.7
			3	2.17	0.6956	31.6	54.4	54.2
	20	40	0	3.95	0.8615	26.6	10.8	31.8
			3	3.55	1.0690	36.0	62.8	53.3
Average:			0	2.53	0.7123	37.1	16.5	37.6
			3	2.29	0.8413	38.1	59.5	60.7

10 Annex V: Reference Frame Transformation

10.1 Attitude correction

Using three transformation matrices (Eq. 20-22) for all three axes (x, y, z), the pitch (θ), roll (ϕ), and yaw (ψ) angles of the drone will correct the sensor wind measurements for the attitude.

$$T_x(\phi) = \begin{bmatrix} 1 & 0 & 0 \\ 0 & \cos(\phi) & -\sin(\phi) \\ 0 & \sin(\phi) & \cos(\phi) \end{bmatrix} \tag{20}$$

$$T_y(\theta) = \begin{bmatrix} \cos(\theta) & 0 & \sin(\theta) \\ 0 & 1 & 0 \\ -\sin(\theta) & 0 & \cos(\theta) \end{bmatrix} \tag{21}$$

$$T_z(\psi) = \begin{bmatrix} \cos(\psi) & -\sin(\psi) & 0 \\ \sin(\psi) & \cos(\psi) & 0 \\ 0 & 0 & 1 \end{bmatrix} \tag{22}$$

Thereafter, $u, v,$ and w wind components are obtained from the sensor $w_x, w_y,$ and w_z wind measurements using Eq. 23.

$$w_{xyz} = \begin{bmatrix} w_x\ w_y\ w_z \end{bmatrix}$$
$$W_{uvw} = w_{xyz} \cdot T_x(\phi) \cdot T_y(\theta) \cdot T_z(\psi) \tag{23}$$

10.2 Motion correction

$u, v,$ and w wind components will have to be corrected for the motion of the drone, as any movement of drones is registered as wind. First, the drone motions in the East, North, and up directions are determined by simple trigonometry using the drone's vertical speed (v_z), horizontal speed (v_{xy}) and course (φ) using Eq. 24.

$$v_e = v_{xy} \cdot \sin(\varphi)$$
$$v_n = v_{xy} \cdot \cos(\varphi) \tag{24}$$
$$v_u = v_z$$

The actual wind vectors are then obtained by adding the motion to the measured wind using Eq. 25.

$$w_u = w_u + v_e$$
$$w_v = w_v + v_n \tag{25}$$
$$w_w = w_w + v_u$$

11 Annex VI: Ordinary Least Squares Regression Analysis

In brief, an OLS compares the difference between individual points in a data set and the predicted line of best fit to measure the amount of error produced (Hashem, 2015). As implied by the name, a linear regression model assumes that the relationship between the independent variables and dependent variable are linear, as opposed to exponential. In addition, an OLS analysis is extremely sensitive to outliers (Wen et al., 2013). For this analysis, the obstacles (categorical), altitudes (numerical), triangle sizes (numerical) and average wind speeds (numerical) are considered to model the relationship between these independent variables and the dependent wind magnitude and angular errors.

Table 11: Multivariate OLS regression analysis overview to statistically analyse the effect of wind speed on the wind magnitude and angular errors

Dependent variable	Independent variable	Coefficient	Standard error	t	p-value
Vertical angular MAE $Adj. R^2 = 0.689$	Trailer	6.77	3.62	1.87	0.082
	Tree line	12.86	3.70	3.47	0.003
	Altitude	0.02	0.06	0.28	0.784
	Triangle size	0.16	0.08	2.04	0.060
	Wind speed	-4.48	1.30	-3.42	0.004
Horizontal angular MAE $Adj. R^2 = 0.233$	Trailer	0.35	4.38	0.08	0.937
	Tree line	-3.82	4.47	-0.85	0.406
	Altitude	-0.003	0.07	-0.04	0.986
	Triangle size	0.09	0.10	0.93	0.369
	Wind speed	-3.58	1.58	-2.26	0.039
Wind magnitude MAE $Adj. R^2 = 0.154$	Trailer	0.05	0.10	0.51	0.616
	Tree line	0.05	0.11	0.49	0.630
	Altitude	-0.002	0.002	-1.48	0.159

				1.2 6	
	Triangle size	0.003	0.002	1.2 6	0.227
	Wind speed	0.04	0.04	1.1 5	0.267

The results of the OLS analysis are presented in Table 11. For the vertical angular MAE, the adjusted R-squared value is 0.689, which indicates that ~69% of the change in the dependent variable is explained by the changes of the used independent variables (Hashem, 2015). Cautiously adhering to $p < 0.05$ as a rejection rule of the null hypothesis (Dahiru, 2008), the p-value of 0.004 states that there is a 0.4% chance that the wind speed has no effect on the vertical angular error. Therefore, it is very likely that the low wind speeds during the experiment day have a significant negative effect on the error, where a decrease of 1 m/s in wind speed corresponds to a 4.48° error increase. Despite having a low adjusted R-squared value, the average wind speed also seems to have some significance given the horizontal angular MAE. In contrast, the independent variables show no statistical significance for the 3D wind magnitude MAE. Furthermore, the *condition number* of the regression analysis is 224. A condition number is a measurement of the sensitivity of the model as compared to the size of changes in the data it is analysing (Hashem, 2015). Multicollinearity is strongly implied by a condition number > 30. Multicollinearity is a term to describe a high degree of intercorrelations among the independent variables in a multivariate regression equation (Hashem, 2015). The independent variables might interact with each other. By studying the interaction effects of multiple independent variables, it can indicate a probable third variable which influences the relationship between an independent and dependent variable (Frost, 2021). This would be critical to incorporate in the model, but lies beyond this study and could be implemented in future research.

As mentioned above, a linear regression analysis assumes there is a linear relationship, as opposed to an exponential relationship. In addition, an OLS analysis is extremely sensitive to outliers (Wen et al., 2013). This regression analysis cannot be used as ground truth. Nonetheless, it implies that the average wind speed only affects the angular errors.